Article:

Hofstra, M, Peakall, J, Hodgson, DM orcid.org/0000-0003-3711-635X et al. (1 more author) (2018) Architecture and morphodynamics of subcritical sediment waves in an ancient channel–lobe transition zone. Sedimentology, 65 (7). pp. 2339-2367. ISSN 0037-0746

https://doi.org/10.1111/sed.12468

Architecture and morphodynamics of subcritical sediment waves in an ancient channel-lobe transition zone

M. Hofstra[1]†, J. Peakall[1], D.M. Hodgson[1], C.J. Stevenson[2]

[1]*Stratigraphy Group, School of Earth and Environment, University of Leeds, Leeds, LS2 9JT, UK*

[2]*School of Earth, Ocean and Ecological Sciences, University of Liverpool, L69 3GP, UK*

†*corresponding author [Email: menno.hofstra.1@gmail.com]*

Running title: Subcritical sediment wave architecture in a CLTZ

Keywords: channel-lobe transition; subcritical; sediment wave; base-of-slope; Karoo Basin; facies characteristics; process record

ABSTRACT

In modern systems, submarine channel-lobe transition zones (CLTZs) show a well-documented assemblage of depositional and erosional bedforms. In contrast, the stratigraphic record of CLTZs is poorly constrained, because preservation potential is low, and criteria have not been established to identify depositional bedforms in these settings. Several locations from an exhumed fine-grained base-of-slope system (Unit B, Laingsburg depocentre, Karoo Basin) show exceptional preservation of sandstone beds with distinctive morphologies and internal facies distributions. The regional stratigraphy, lack of a basal confining surface, wave-like morphology in dip section, size, and facies characteristics support an interpretation of subcritical sediment waves within a CLTZ setting. Some sediment waves show steep (10-25°) unevenly spaced (10-100 m) internal truncation surfaces that are dominantly upstream-facing, which suggests significant spatio-temporal fluctuations in flow character. Their architecture indicates individual sediment wave beds accrete upstream, in which each swell initiates individually. Lateral switching of the flow core is invoked to explain the sporadic upstream-facing truncation surfaces, and complex facies distributions vertically within each sediment wave. Variations in bedform character are related to the axial to marginal positions within a CLTZ. The depositional processes documented do not correspond with known bedform development under supercritical conditions. The proposed process model departs from established mechanisms of sediment wave formation by emphasising the evidence for subcritical rather than supercritical conditions, and highlights the significance of lateral and temporal variability in flow dynamics and resulting depositional architecture.

INTRODUCTION

Bedforms are rhythmic features that develop at the interface of fluid flow and a moveable bed (e.g. Southard, 1991; Van der Mark *et al.,* 2008; Baas *et al.,* 2016). Sediment waves are a type of long wavelength (tens of ms to kms) depositional bedform that vary in grain size from mud- to gravel-dominated, linked to their depositional setting (Fig. 1) (Wynn & Stow, 2002). They have been identified in numerous modern channel-lobe transition zones (CLTZs) (Normark & Dickson, 1976; Damuth, 1979; Lonsdale & Hollister, 1979; Normark *et al*., 1980; Piper *et al*., 1985; Malinverno *et al*., 1988; Praeg & Schafer, 1989; Howe, 1996; Kidd *et al*., 1998; Morris *et al*., 1998; McHugh & Ryan, 2000; Migeon *et al*., 2001; Normark *et al*., 2002; Wynn & Stow, 2002; Wynn *et al*., 2002a,b; Heiniö & Davies, 2009), where they form part of a distinctive assemblage of depositional and erosional bedforms (Mutti & Normark, 1987, 1991; Normark & Piper, 1991; Palanques *et al*., 1995; Morris *et al*., 1998; Wynn *et al*., 2002a,b; Macdonald *et al*., 2011). However, the detailed sedimentological and stratigraphic record of sediment waves from CLTZ and channel-mouth settings is not widely documented.

Vicente Bravo & Robles (1995) described hummock-like and wave-like depositional bedforms from the Albian Black Flysch, NE Spain. The hummock-like bedforms (5 to 40 m wavelength and a few decimetres to 1.5 m high) were interpreted to be genetically related to local scours. The wave-like bedforms (5 and 30 m wavelength and a few cm to 0.7 m high) seen in longitudinal sections exhibit symmetric to slightly asymmetric gravel-rich bedforms. Ponce & Carmona (2011) identified sandy conglomeratic sediment waves with amplitudes up to 5 m and wavelengths ranging between 10 to 40 m at the northeast Atlantic coast of Tierra del Fuego, Argentina. Ito *et al*. (2014) described medium- to very coarse-grained sandstone tractional structures from a Pleistocene canyon-mouth setting within the Boso Peninsula, Japan, with wavelengths up to 40 m and crest heights up to 2 m. These coarse-grained examples from Japan, Argentina, and Spain lack detailed internal facies descriptions and structure. Data on long wavelength finer-grained sediment waves in the rock record are largely missing (Fig. 1), ascribed to their wavelength and poor exposure potential (Piper & Kontopoulos, 1994). Modern examples that are dominantly fine grained (silt to mud) and show substantial wavelengths (Fig. 1) are typically interpreted as large supercritical bedforms (Symonds *et al*., 2016), similar to cyclic steps. This is due to observations from geophysical data of their short lee-sides and long depositional stoss-sides, and apparent single bedform structures with upstream sediment wave migration as a sinusoidal wave (Cartigny *et al*., 2014; Hughes-Clark, 2016; Covault *et* *al*., 2017). Indeed, upstream migration of sediment waves is taken as an indicator of bedform evolution under supercritical flow conditions (Symonds *et al*., 2016). However, the processes responsible for the inception and morphological evolution of sediment waves within CLTZ settings remain poorly constrained, and high-resolution observations of their sedimentology are needed to explore the balance of subcritical and supercritical processes in their inception, evolution, and depositional record.

Here, we aim to improve understanding of sediment wave development in CLTZs through studying multiple stratigraphic sections from well-constrained base-of-slope systems (Unit B, Laingsburg depocentre, Karoo Basin) where distinctive fine to very-fine-grained sandstone depositional bedforms with complex architecture, facies and stacking patterns are exposed. The objectives are: 1) to document and interpret the depositional architecture and facies patterns of these sandstone bedforms, 2) to discuss the topographic controls on their inception, 3) to propose a process model for sediment wave development under subcritical rather than supercritical flow conditions, and, 4) to consider the controls on the preservation potential of sediment wave fields in channel-lobe transition zones.

REGIONAL SETTING

The southwest Karoo Basin is subdivided into the Laingsburg and the Tanqua depocentres. The Ecca Group comprises a ~2 km-thick shallowing-upward succession from distal basin-floor through submarine slope to shelf-edge and shelf deltaic settings (Wickens, 1994; Flint *et al*., 2011). The deep-water deposits of the Karoo Basin have a narrow grain size range from clay to upper fine sand. Within the Laingsburg depocentre (Figs 2A and 3A), Unit B, the focus of this study, is stratigraphically positioned between underlying proximal basin-floor fan deposits of Unit A (e.g. Sixsmith *et al*., 2004; Prélat & Hodgson, 2013) and the overlying channelised slope deposits of the Fort Brown Formation (Unit C-G; e.g. Hodgson *et al*., 2011; Van der Merwe *et al*., 2014). Unit B comprises a 200 m thick section at the top of the Laingsburg Formation (Grecula *et al*., 2003; Flint *et al*., 2011; Brunt *et al*., 2013), and is subdivided in three subunits, B1, B2 and B3 (Fig. 3A; Flint *et al*., 2011; Brunt *et al*., 2013). Unit B is well-exposed for more than 350 km^2 providing both down dip and across strike control (Brunt *et al*., 2013) with over 15 km long exposed sections along the limbs of the Baviaans and Zoutkloof synclines and Faberskraal anticline (Fig. 2A). The study area is situated between well-defined up-dip slope channels and down-dip basin-floor lobes (Figs 3B and 3C; Grecula *et al*., 2003; Pringle *et al*., 2010; Brunt *et al*., 2013). Therefore, the palaeogeographic setting is interpreted to be a base-of-slope setting, where CLTZ-elements are more likely to be preserved (Figs 3B and 3C).

METHODOLOGY AND DATASET

Two areas of Unit B exposure were studied in detail: one located in the southern limb of the Zoutkloof Syncline (Doornkloof) and one located in the southern limb of the Baviaans Syncline (Old Railway) (Fig. 2). Stratigraphic correlations using closely-spaced sedimentary logs (m's to tens of m's), photomontages, and walking out key surfaces and individual beds with a handheld GPS enabled construction of architectural panels. Where the exposure allowed collection of sub-metre-scale sedimentary logs individual beds were correlated over multiple kilometres. Within the Doornkloof area (Fig. 2B) 11 long (>20-200 m) sedimentary logs, supported by 31 short (<5 m) detailed sedimentary logs, were collected along a 2 km long E-W section. Particular emphasis was placed on bed-scale changes in facies to construct detailed correlation panels. Additionally, a research borehole drilled 330 m north of the studied outcrop section (DK01; 460983-6331775 UTM; Hofstra, 2016) intersected the lower 92 m of Unit B (Figs 2A and 2B). Within the Old Railway area (Fig. 2C), eight short and closely spaced (5-20 m distance) detailed sedimentary sections were collected. Palaeocurrents were collected from ripple-laminated bed tops and re-orientated, with 117 palaeoflow measurements at Doornkloof and 87 from the Old Railway area.

FACIES AND ARCHITECTURE

Both study areas contain sandstone-prone packages that comprise bedforms with substantial downdip thickness and facies changes without evidence for confinement by an incision surface. The rate of thickness change and the range of sedimentary facies are markedly different from that documented in basin-floor lobes (e.g. Prélat & Hodgson, 2013). Bed thicknesses change (metre scale) in a downstream-orientated direction on short spatial-scales (tens of metres), compared to lateral continuous bed thickness (hundreds of metres) known from lobes (e.g. Prélat *et al*., 2010). Similarly, facies change markedly over metre scales, in contrast to lobes where facies changes are transitional over hundreds of metres (e.g. Prélat *et al*., 2009). Depositional bedforms in both study areas are present within a sandstone-prone (>90%) package of dominantly medium-bedded structured sandstones, interbedded with thin-bedded and planar-laminated siltstones. The grain size range is narrow, from siltstone to fine-grained sandstone, with a dominance of very-fine-grained sandstone.

Facies characteristics

The sedimentary facies within the bedforms are subdivided into four types: structureless (F1), banded to planar-laminated (F2), small-scale bedform structures (F3), and mudstone clast conglomerates (F4).

F1: Structureless sandstones show minimal variation or internal structure and are uniform in grainsize (fine-grained sandstone). Locally, they may contain minor amounts of dispersed sub-angular mudstone clasts (1-10 cm in diameter) and flame structures at bed bases.

Interpretation: These sandstones are interpreted as rapid fallout deposits from sand rich high-density turbidity currents (Kneller & Branney, 1995; Stow & Johansson, 2000; Talling *et al*., 2012) with mudstone clasts representing traction-transported bedload. Flame structures at the bases of structureless beds are associated with syn-depositional dewatering (Stow & Johansson, 2000).

F2: Banded and planar-laminated sandstones show large variations in character. The differentiation between planar-laminated and banded facies is based on the thickness and character of the laminae or bands. In banded sandstones, the bands are 0.5-3 cm thick and defined by alternations of clean sand bands, and dirty sand bands rich in mudstone clasts and/or plant fragments. Planar-laminations show <1 cm thick laminae that are defined by clear sand-to-silt grain-size changes. Furthermore, bands can be wavy or convolute, show substantial spatial thickness variations (<1 cm) at small (<1 m) spatial scales, and exhibit subtle truncation at the bases of darker bands. Banded facies are mudstone clast-rich where close to underlying mudstone clast conglomerates. In some places, banded sandstone beds can be traced upstream into mudstone clast conglomerates. Where this facies is observed, bed thicknesses typically exceed 0.5 m.

Interpretation: Planar-lamination and banding are closely associated, and in many cases are difficult to distinguish. This suggests that their depositional processes are closely related and are therefore combined here into a single facies group. Planar laminated sandstones can be formed under dilute flow conditions via the migration of low-amplitude bedwaves (Allen, 1984; Best & Bridge, 1992), or under high-concentration conditions from traction carpets (Lowe, 1982; Sumner *et al*., 2008; Talling *et al*., 2012; Cartigny *et al*., 2013). The banded facies may be formed as traction carpet deposits from high-density turbidity currents and are comparable to the Type 2 tractional structures of Ito *et al*. (2014) and the H2 division of Haughton *et al*. (2009). Deposits related to traction carpets can show significant variation in facies characteristics (e.g. Sohn, 1997; Cartigny *et al*., 2013). Alternatively, the banded facies may represent low-amplitude bedwave migration that formed under mud-rich transitional flows (Baas *et al*., 2016).

F3: Fine-grained sandstones with decimetre-scale bedform structures. The majority (~80%) of this facies is represented by climbing ripple-lamination, commonly with stoss-side preservation. Locally, small-scale (wavelengths of decimetre-scale, and heights of a few cm) bedforms are present that show convex-up laminae, biconvex tops, erosive to non-erosive basal surfaces, and laminae that can thicken downwards (Figs 4A and 4C). In some cases, the bedforms show distinct low-angle climbing (Fig. 5A). Isolated trains of decimetre-scale bedforms are present between banded/planar-laminated facies (Figs 4B and 4C), whereas those exhibiting low-angle climbing can form above banded/planar-laminated sandstone and in some cases transition into small-scale hummock-like features (Fig. 4A). These hummock-like bedforms consist of erosively based, cross-cutting, concave- and convex-up, low- to high-angle (up to 25°) laminae sets (Fig. 4A). They have decimetre to centimetre wavelengths, and amplitudes up to 10 cm. Locally, internal laminae drape the lower bounding surfaces and these tend to be low angle surfaces, whereas elsewhere laminae downlap onto the basal surface, typically at higher angles (Fig. 4A). Where laminae are asymmetric they have accreted in a downslope direction.

Furthermore, sinusoidal laminations are observed (Fig. 4A) with exceptional wavelengths (>20 cm) and angles-of-climb (>45°) in comparison to conventional stoss-side preserved climbing ripples (15-45°; 10-20 cm). These features also differ from convolute laminae/banding as they do show a consistent wavelength and asymmetry. However, it is difficult to consistently make clear distinctions between stoss-side preserved ripples and sinusoidal laminations. Hence, they are grouped together into 'wavy bedform structures'.

F3 facies is most common at bed tops, but is also observed at bed bases, where laterally they are overlain by an amalgamation surface. Locally, mudstone clasts (<1-4 cm) have been observed within ripple-laminated segments.

Interpretation: Climbing ripple-lamination is interpreted as high rates of sediment fallout with tractional reworking from flows within the lower flow regime (Allen, 1973; Southard & Boguchwal, 1990). The mudstone clasts are interpreted to be the result of overpassing of sediments on the bed (Raudkivi, 1998; Garcia, 2008). When sedimentation rate exceeds the rate of erosion at the ripple reattachment point, the stoss-side deposition is preserved and aggradational bedforms develop (Allen, 1973). This is indicative of high rates of sediment fallout (Jopling & Walker, 1968; Allen, 1973; Jobe *et al*., 2012), attributed to rapid flow deceleration from moderate-to-low concentration turbidity currents (Allen, 1973). Sinusoidal lamination is interpreted as a type of climbing ripple lamination, marked by very high sedimentation rates, leading to similarity in thickness between stoss and lee sides (Jopling & Walker, 1968; Allen, 1973; Jobe *et al.*, 2012).

The more convex bedforms (Figs 4A and 4C) bear similarities with washed out ripples that are formed under high near-bed sediment concentration conditions at the transition from ripples to upper stage plane beds in very fine sands (Baas & de Koning, 1995), and with combined-flow ripples that have rounded tops and convex-up lee slopes (Harms, 1969; Yokokawa *et al*., 1995; Tinterri, 2011). In turbidites, these bedforms have been termed 'rounded biconvex ripples with sigmoidal laminae', and have been associated with reflected flow facies where turbidity currents have interacted with topography (Tinterri, 2011; Tinterri & Muzzi Magalhaes, 2011; Zecchin *et al*., 2013; Tinterri & Tagliaferri, 2015). A third possibility is that these are decimetre-scale stable antidunes since these can exhibit biconvex tops and in some cases convex-up cross-lamination (Alexander *et al*., 2001; Cartigny *et al*., 2014; Fedele *et al*., 2017), although these bedforms may also frequently show concave laminae (Cartigny *et al*., 2014). Typically, antidune laminae dip upstream (e.g., Alexander *et al*., 2001; Cartigny *et al*., 2014), although downstream migrating antidunes are known from both open-channel flows (e.g., Kennedy, 1969) and gravity currents (Fedele *et al*., 2017).

The 'hummocky-type' structures (Fig. 4A) with high-dip angles (up to 25°), draping of laminae, and limited variation in laminae thickness, show similarities with anisotropic hummocky cross stratification (HCS) from combined oscillatory-unidirectional flows (e.g., Dumas *et al*., 2005; Dumas & Arnott, 2006). Maximum dip angles of laminae in strongly anisotropic HCS can be around 25-30° (Dumas *et al*., 2005; Dumas & Arnott, 2006) much higher than for symmetrical forms, which are typically less than 15° (Harms *et al*., 1975; Tinterri, 2011). However, thickening and thinning of laminae are expected in HCS (Harms *et al*., 1975) and are not clearly observed in the hummocky-like bedforms here. Such HCS-like hummocky bedforms have been interpreted from basin plain turbidites to be related to reflected flows from topographic barriers (Tinterri, 2011; Tinterri & Muzzi Magalhaes, 2011). Hummock-like bedforms in turbidites have also been interpreted as antidunes (e.g., Skipper, 1971; Prave & Duke, 1990; Cartigny *et al*., 2014). Antidunes are typically associated with concave upward erosive surfaces, extensive cross-cutting sets if they are unstable antidunes, bundles of upstream dipping laminae (if upstream migrating), laminae with low dip angles, low angle terminations against the lower set boundary, some convex bedding, and structureless parts of fills (e.g., Alexander *et al*., 2001; Cartigny *et al*., 2014; Fedele *et al*., 2017). The hummock-like bedforms in the present study share many similarities with these antidunes, however there is an absence of structureless components, the draping of surfaces is more pronounced and more typical of HCS, the approximately parallel nature of laminae within sets is more pronounced and the number of laminae is greater. Furthermore, set bundles accrete downstream suggesting that if these are antidunes then they are downstream-migrating forms. In summary, the hummock-like bedforms show greater similarity to those HCS-like structures described from reflected flows (Tinterri, 2011; Tinterri & Muzzi Magalhaes, 2011), rather than features associated with downstream migrating antidunes.

The observed combination of biconvex ripples and anisotropic hummock-like features, and the transitions between these bedforms in some vertical sections, is also in agreement with that observed in some turbidity currents interacting with topography (Tinterri, 2011; Tinterri & Muzzi Magalhaes, 2011), further suggesting that the hummock-like features may be related to combined flows, rather than the product of antidunes. This possibility of topographic-interaction induced hummock-like and biconvex ripple forms is discussed further, after the topography of the sediment waves is introduced.

F4: Mudstone clast conglomerate deposits form discrete patches (<20 m long and <0.3 m thick), which commonly overlie erosion surfaces. Mudstone clasts (<1 cm – 10 cm diameter) vary from subangular to well-rounded. They are dominantly clast supported with a matrix of fine-grained sandstone.

Interpretation: Mudstone clast conglomerates are interpreted as lag deposits (e.g. Stevenson *et al*., 2015) from energetic and bypassing high-density turbidity currents.

Bed architecture and facies distribution: Doornkloof – Subunit B1

At Doornkloof (Fig. 2), subunit B1 has an average thickness of ~5 m (Fig. 5) and comprises thin- to thick-bedded sandstones, thin-bedded siltstones and lenticular mudstone clast conglomerates (0.1-0.3 m thick, 1-70 m wide) (Figs 5 and 6A-E). There are substantial variations in bed thicknesses and sandstone-to-siltstone proportions along the 1.5 km long dip section (Fig. 5). Locally, medium- to thick-bedded sandstones occur, which comprise bedforms within a package of thin-bedded siltstones and sandstones. These bedforms show regional changes to more tabular thin-bedded sandstones and siltstones (log 01/log 08, Fig. 5). Within the exposed section (~ 2 km), there are three sandstone-prone bedform-dominated sections (200 m to 300 m in length) separated by siltstone-prone sections (150 to 400 m in length), which have an overall tabular appearance (Fig. 6). The DK01 core (Figs 5 and 6) is located 330 m to the north of the western limit of Section I where subunit B1 is a ~5 m thick package of interbedded thin structured sandstones and laminated siltstones (Fig. 6). Multiple erosion surfaces are present at the base, and overall in the DK01 core the subunit B1 succession fines- and thins-upward. Palaeoflow of the B1 subunit is dominantly ENE-orientated (082°) (Fig. 2B) but shows some deviation within the eastern part of the section (log 42 – Figs 2B and 5) towards the NNE (023°).

The medium- to thick-bedded sandstones within the sandstone-prone sections of Section I, orientated (079°-259°) subparallel to palaeoflow, show large lateral variations in thickness and facies. The bedforms comprise structureless (F1), planar-laminated to banded (F2), and ripple-laminated (F3) sandstones (Fig. 6A-E). The facies, architecture and thickness changes of one amalgamated bed (*Bedform a*) are described in detail (Fig. 5). *Bedform a* thickens (up to 2.5 m) and thins (<20 cm) multiple times, forming a down-dip pinch-and-swell morphology. Locally, the base of *Bedform a* is marked by shallow erosion (<0.5 m deep; <30 m long) and in some places is amalgamated with the underlying sandstone beds (Figs 5 and 7). Where *Bedform a* exceeds 0.5 m in thickness, banded (F2) sandstone facies is dominant, and is in some places underlain by structureless (F1) divisions, or exhibits climbing ripple-lamination at the bed top (F3). Where *Bedform a* is thin (<0.5 m thick), it is dominated by climbing-ripple lamination (F3). Below *Bedform a,* lenses of mudstone conglomerate

(<30 m long; 5-30 cm thick) can be observed at various locations over the complete section. In some locations (e.g. log 16/18, Fig. 5), banded sandstone (F2) beds (Fig. 6D) can be observed intercalated with mudstone clast conglomerate lenses (Fig. 7). These banded beds pinch out or show a transition towards mudstone clast conglomerates upstream, and are amalgamated with *Bedform a* downstream. At the same stratigraphic level as *Bedform a*, the DK01 core shows one pronounced 20 cm thick bed with angular mudstone clasts (<1-5 cm diameter) that can be correlated to *Bedform a*.

In *Bedform a,* six truncation surfaces (10-25°) are identified within the eastern limit of the section (Fig. 5), at places where the bedform exceeds 1 m in thickness. All truncation surfaces are sigmoid-shaped and flatten out upstream and downstream within the bed (Fig. 6E). One eastward (downstream) orientated truncation surface (Fig. 6B) in the lower part of the bed is observed at log 17 (Fig. 5). However, sigmoidal westward (upstream) facing truncation surfaces are most common in the upper portion of the bed and are spaced 15-20 m apart. They cut banded (F2) and ripple-laminated (F3) sandstone facies, and are sharply overlain by banded sandstone facies (F2) with bands aligned parallel to the truncation surface, or by climbing-ripple laminated segments (Fig. 6E). Abrupt upstream thinning (SW) and more gradual downstream thickening (NE) give *Bedform a,* an asymmetric wave-like morphology in dip section. Small-scale bedforms (F3) are solely present at the top of the wave-like morphology, and dominantly comprise climbing-ripple lamination, with occasional wavy bedforms (stoss-side preserved climbing ripples and/or sinusoidal laminations) at the thicker sections of the bedform (Fig. 5). At abrupt bed thickness changes associated with steep westward-facing truncation surfaces (>15°) (logs 16/19/21, Fig. 5), shallow scour surfaces (<0.35 cm) can be observed that cut into the top surface of *Bedform a*, overlain and onlapped by thin-bedded siltstones and sandstones. Within the banded facies (F2), isolated lenses of ripple-lamination (F3) are present (up to 30-40 cm long and 10 cm thick) (Fig. 5 – log 19). Mudstone and siltstone clasts (0.2-5 cm diameter) dispersed throughout structureless (F1) sections are typically well rounded, and rarely sub-angular. At the eastern limit of Section I, stratigraphically below *Bedform a*, another ‘pinch-and-swell’ sandstone bed abruptly increases in thickness downstream where *Bedform a* is amalgamated with this bed below (log 21, Fig. 5). Where the bed thickens, *Bedform a* thins abruptly (log 23/24, Fig. 5). The thin-bedded and siltstone-prone deposits overlying *Bedform a* show more laterally constant geometries, thicknesses and facies.

At the upstream end (SW) of Section 1, around log 02-07 (Fig. 5, middle panel), a package of sandstone beds thickens locally (>100 m long, <5 m thick) above *Bedform a* (Fig. 8). *Bedform a* pinches and swells multiple times within this log 02-07 interval to a maximum of 0.5 m thickness and comprises similar facies as downstream (F1, F2, F3), but lacks internal truncation surfaces. The bed directly above *Bedform a* thickens where *Bedform a* thins and *vice versa* (Fig. 8). Sandstone beds above both this bed and *Bedform a*, in the top of the package, show only limited thickness variations (~10 cm) and dominantly comprise climbing ripple-laminated sandstone (F2). All sandstone beds above *Bedform a* either pinch-out or show a facies transition towards fine siltstone in both western and eastern directions (Fig. 5).

Bed architecture and facies distribution: Doornkloof – Subunit B2

The sandstone bed morphology and facies characteristics at the base of subunit B2 share many affinities with the deposits described within subunit B1 (Fig. 9). Palaeoflow of subunit B2 is generally NE-orientated (040°) (n=68; Figs 2B and 9B) but with a high degree of dispersion, and a shift from ENE (062°) in the western part of the section, to more northwards in the middle (19°) and eastern part of the section (030°). This indicates that the section is dominantly subparallel to palaeoflow (dip section) (Fig. 2B). Subunit B2 dominantly comprises medium-bedded (0.1-0.5 m thick) structured sandstone (Fig. 9B). Closely spaced logs (m’s to tens of m’s) collected from the main face at the base of B2 (Section II – Fig. 2B) permit tracing out of individual beds over a distance of 230 m and tracking of internal facies changes (Fig. 6F-J). Two beds (*Bedform b* and *Bedform c*) change in thickness (0.5-2 m for *Bedform b* and 0.3-1.2 m for *Bedform c*) and contain multiple internal truncation surfaces of which six are westward (upstream) facing and one is eastward (downstream) facing. Truncation surfaces cut climbing ripple-laminated facies (F3) and banded facies (F2) with maximum angles varying between 20-30° that shallow out and merge with the base of the bed (Figs 6G, 6H and 6J). They flatten out in the downstream direction within the bed and are overlain by banded sandstone facies (F2). In *Bedform b*, the rate of westward thinning is more abrupt than eastward, giving an asymmetric wave-like morphology (Fig. 9B). This abrupt westward thinning is coincident with locations of westward (upstream) orientated truncation surfaces. In the eastern part, 110 m separates two truncation surfaces, in an area associated with bed thinning. However, towards the western part of *Bedform b*, there is only 25-30 m between the westward (upstream) orientated truncation surfaces, with no abrupt bed thinning.

There is a high degree of longitudinal and vertical facies variability within *Bedform b* and *c* (Figs 4 and 9B). Commonly, longitudinal facies changes are accompanied by bed thickness changes. Locally, the bases of thicker parts of the bedforms are mudstone clast-rich. Bed tops show small-scale bedform structures (F3) at most locations. Banded sandstone facies overlie the truncation surfaces (Figs 6G, 6H and 6J). Ripple-laminated facies (F3) within the middle or lower parts of *Bedform b* and *c* indicate flow directions that deviate (NW to N) from the regional palaeoflow (NE) (Figs 4A, 6F and 6H), whereas the palaeoflow direction of the ripples at the top of the bedforms are consistent with the regional palaeoflow. Detailed analysis of well-exposed sections (Fig. 4) indicates that many laminated and banded sections are wavy and separated by low angle truncation or depositional surfaces. Locally, small-scale bedform structures (F3) are present in patches (Figs 4B and 4C) (<10 cm thick; couple of metres wide), which show downstream and/or upstream facies transitions to banded/planar-laminated facies (F2), as well as examples of flame structures (Fig. 4C). The small-scale bedform structures (F3) show a lot of variability, with hummock-like features observed above biconvex ripples at both the downstream end of swells, and directly below truncation surfaces at the upstream end of swells (Fig. 4A). Additionally, both hummock-like features and biconvex ripples have been observed at the base of *Bedform* b (log 38; Fig. 9B). Similar to *Bedform a*, *Bedform b & c* show wavy bedform structures at the top of swells, particularly where they are the thickest. *Bedform b* is topped in the easternmost exposure by a scour surface that cuts at least 0.5 m into *Bedform b* and is amalgamated with an overlying pinch-and-swell sandstone bed (Fig. 9B). Medium- to thin-bedded structured sandstones are present above and below *Bedform b* and *c*, which do not show any facies or thickness changes over the exposed section.

The basal succession of subunit B2 in the DK01 core, at the same stratigraphic level as *Bedform b* and *c*, comprises thick-bedded structureless (F1) to banded (F2) (>3 m) sandstones. Bed bases are sharp and structureless and contain a variable amount of mudstone clasts (<1 cm). The middle to upper parts of these beds show banded facies (F2) with clear mudstone clast-rich and -poor bands, which pass through wavy lamination to climbing ripple (F3) and planar lamination at bed tops.

Above Section II, in both outcrop and core, a 15 m thick sandstone package shows a substantial increase in bed thicknesses (max. 4.5 m), mainly due to bed amalgamation (Fig. 9A). Some of these beds show a wave-like (asymmetric) morphology, similar to that observed in *Bedforms b and c.* Abrupt bed thinning or pinch-out is common. These pinch-outs are primarily associated with depositional geometry, with rare examples of bed truncation by erosion surfaces. Bounding surfaces can be identified within the sandstone package, which are defined by successive upstream depositional bed pinch-out points (Fig. 10), with local (<2 m long) shallow (<0.3 m) erosion surfaces. These bounding surfaces separate multiple packages of downstream shingling (three to four) sandstone beds. The packages of pinch-and-swell beds are stacked in an aggradational to slightly upstream orientated manner (Fig. 10) and are topped by a >60 m thick package of tabular and laterally continuous medium- to thin-bedded structured sandstones. At the same interval in the DK01 core a transition can be observed from thick- to medium-bedded, dominantly banded (F2), sandstones towards more medium- to thin-bedded structured (F3) sandstones.

Bed architecture: Old Railway – Subunit B2

At this locality on the southern limb of the Baviaans Syncline, the lower 10 m of subunit B2 is exposed for 100 m EW (Fig. 2C). Here, B2 is a medium- to thin-bedded sandstone-prone unit that shows substantial lateral thickness changes without evidence of a basal erosion surface (Fig. 11).

Mean palaeoflow is ESE (121°) (Fig. 2C), indicating the exposure is sub-parallel to depositional dip. The sandstone beds are dominantly climbing ripple laminated (F3), with some banded/planar laminated (F2) and structureless divisions (F1).

Multiple climbing ripple laminated beds contain dispersed small mudstone and siltstone clasts (Fig. 11C). The section is characterised by an alternation of beds showing typical pinch-and-swell geometries (0.5-2 m) and more tabular thin-bedded (<0.5 m) sandstones. Locally, individual beds pinch-and-swell multiple times over a distance of ~40 m, with wavelengths varying from 15 m to >40 m. Where there are swells, bed bases truncate underlying beds (Fig. 11D). Siltstones comprise only ~10% of the succession and are thin-bedded and planar-laminated, with intercalated thin very fine-grained sandstones (<1 cm).

Towards the top of the section, a 40 cm thick very fine-grained sandstone bed abruptly fines and thins downstream to a centimetre-thick siltstone bed (Fig. 12). This bed thickens and thins along a ~20 m distance (Fig. 12) forming sandstone lenses, before regaining original thickness (40 cm). Locally, within this zone, the bed longitudinally grades to siltstone and is perturbed from the top by decimetre-scale scour surfaces (0.2-3 m long, couple of cm’s deep). At log 04 (Fig. 11A), a bed that pinches downstream has a downstream-orientated scour on its top surface, which is overlain by thin-bedded sandstones and siltstones that pass upstream beyond the confines of the scour surface. A downstream thickening bed with an erosive base truncates these beds. The majority of the observed pinch-and-swell bedforms stack in a downstream direction (Fig. 11A). However, in the middle of the package at log 1, one bed stacks in an upstream manner, giving the overall package an aggradational character. This is similar to the stacking patterns observed within subunit B2 at the Doornkloof section (Fig. 10).

Sediment waves within channel-lobe transition zones

The Doornkloof and Old Railway sections show bedforms with clear pinch-and-swell morphology that are subparallel to flow direction. These bedforms developed in a base-of-slope setting without any evidence of a large-scale basal confining surface. Bed-scale amalgamation and scouring are common in the two study areas, however the more significant component of downstream bed thickness changes is depositional. Their geometry and dimensions (>1 m height; 10-100 m wavelength), support their classification as sediment waves (Wynn & Stow, 2002). The bedforms described from the Doornkloof area (*Beds a-c*) show clear asymmetric pinch-and-swell morphologies, related to internal upstream-facing truncation surfaces (Figs 5 and 9). The well-constrained base-of-slope setting (Brunt *et al*., 2013), the lack of confining erosion surfaces, and the lobe-dominated nature of Unit B downdip (Figs 3B and 3C) are consistent with an interpretation that the sediment waves formed within a CLTZ setting.

DISCUSSION

Topographic control on sediment wave inception

The interpreted CLTZ setting for the sediment waves means that initial deposition is most likely related to flow expansion at the channel-mouth (e.g. Hiscott, 1994a; Kneller, 1995; Mulder & Alexander, 2001). The occurrence of abrupt downstream bedform thickening (e.g. *Bedform a*, Fig. 5), indicates a marked decrease in flow capacity resulting in a temporary increase of deposition rates (e.g. Hiscott, 1994a). Although deposition is expected in areas of flow expansion, this does not explain why sediment wave deposition appears to be localised (e.g. log 02-07; Fig. 5). Both the inception and development of the sediment waves are interpreted to be related to the presence of seabed relief (dm's to m's amplitude). Seabed irregularities are common in base-of-slope settings, and minor defects (such as scours lined with mudstone clast conglomerates; Fig. 7) could have triggered deposition from flows close to the depositional threshold (Wynn *et al*., 2002a). The presence of bedforms overlying swells of older bedforms, such as at the upstream location of *Bedform a* (Figs 5 (logs 2-7) and 8) or the sediment waves overlying *Bedform b* in subunit B2 (Fig. 10), suggest that relief of older bedforms, and consequent flow deceleration, may also act as a nucleus for later sediment wave development. The locally observed decimetre-scale deep scours probably had a more variable effect on sediment wave development. In some cases it resulted in topographic relief that could help sediment wave nucleation (e.g. log 4, Fig. 11) and in other cases the scours remove positive depositional relief (e.g. Fig. 12) and therefore they will have a slight negative effect on sediment wave nucleation. The aggradational character of the sediment wave packages (Figs 10 and 11A) supports a depositional feedback mechanism. Depositional bedforms form positive topography, which may help to nucleate sites of deposition and the development of composite sediment waves forming the complicated larger-scale sediment wave architecture (Figs 10 and 11A).

Bed-scale process record

The sediment wave deposits from CLTZ settings in Unit B are diverse and show significant facies variations on the sub-metre scale. The characteristics of the sediment wave deposits from the two Unit B datasets are discussed and compared.

Bed-scale process record - Doornkloof section

Facies of the sediment waves identified at the Doornkloof section are characterised by an assemblage of structureless (F1), banded and planar laminated (F2), and climbing ripple laminated (F3) sandstones. Local patches of structureless sandstone facies (F1) (Figs 5 and 9B) at bed bases, suggest periods of more enhanced deposition rates (e.g. Stow & Johansson, 2000). However, the sediment waves are dominated by banded facies, likely related either to traction-carpet deposition (Sumner *et al*., 2008; Cartigny *et al*., 2013) or low-amplitude bedwave migration under transitional flows (Baas *et al*., 2016). This suggests deposition from high concentration flows during bedform development. The high degree of F2 variation (band thickness, presence of shallow truncations, wavy nature) is explained by: 1) turbulent bursts interacting with a traction carpet (Hiscott, 1994b); 2) waves forming at the density interface between a traction carpet and the overlying lower-concentration flow, possibly as a result of Kelvin-Helmholtz instabilities (Figs 4 and 6) (Sumner *et al*., 2008; Cartigny *et al*., 2013); 3) the presence of bedwaves and associated development beneath mixed-load, mud-rich, transitional flows (Baas *et al*., 2016), or some combination of these processes. There is a strong spatial and stratigraphic relationship between mudstone clast conglomerates (F4) (Figs 7 and 8) and banded sandstone facies (F2) with a high proportion of mudstone clasts. As the deposits underlying the shallow erosion surfaces are predominantly siltstones, the mudstone clast materials must have been entrained farther upstream, and are therefore interpreted as lag deposits from bypass-dominated high-concentration flows (e.g. Stevenson *et al*., 2015). As scours are typically documented upstream of sediment waves in modern CLTZs (Wynn *et al*., 2002a), the source of these mudstone clasts is likely linked to local upstream scouring, supported by the angularity of the clasts (Johansson & Stow, 1995). The transition from banded facies (F2) to climbing ripple-laminated facies (F3), common at the top of individual beds, likely represents a change from net depositional high concentration flows, to steady deposition from moderate to low concentration flows, and / or a corresponding change from mud-rich transitional flows to mud-poor flows. The dominance of this facies group (F3) at bed tops (Figs 5 and 9B) is interpreted as the product of less-energetic and more depositional tails of bypassing flows.

To understand the process record and evolution of the Unit B sediment waves, it is important to be able to distinguish the record of a single flow event from a composite body comprised of deposits from multiple flow events. The majority of the observed bed thickness changes within the sediment waves at the Doornkloof section are attributed to depositional relief although internally they show steep internal truncation surfaces (Figs 5, 6 and 9). The erosion surfaces may suggest that this depositional architecture is the result of multiple depositional and erosional flow events. However, several lines of evidence suggest these are deposits produced from a single flow event. The preservation of upstream-facing truncation surfaces (Figs 5 and 9B), implies a significant component of bedform accretion at the upstream end (Figs 13 and 14A). To be able to preserve upstream younging truncation surfaces with angles up to 25° (close to the angle-of-repose), the erosion and deposition within each bedform is likely to be the result of a single flow event. Within subunit B2, no bed splitting is observed and all truncation surfaces of *Bedform b* and *c* merge towards the bed base as a single surface (Fig. 9B), leaving underlying strata untouched. This suggests an origin from a single flow event for the entire bedform.

In subunit B1, all upstream facing truncation surfaces in the main sandstone body of *Bedform a* merge onto a single surface within the composite deposit, in a similar manner to *Bedform b* and *c*, further suggesting a single flow origin for the main sediment wave morphology. Additionally, *Bedform a* can be followed out for ~ 1 km in the upstream direction, and shows many small-scale (<5 m longitudinal distance) purely depositional undulations at the western end (Figs 5 and 8). These flow parallel undulations are stratigraphically equivalent to the deposits above the most upstream truncation surface and therefore, represent the youngest depositional phase of *Bedform a* development. The absence of erosion surfaces or bedding planes between these undulations further suggests that the main body of *Bedform a* was formed as a single event bed. The evidence therefore supports the initiation and development of each wave-like bedform in the Doornkloof section (*Bedform a*, *b* and *c*) to be during the passage of a single flow event. Therefore, the internal scour surfaces and bedform undulations are interpreted to be the result of spatio-temporal flow fluctuations from a single flow event. In contrast, the mudstone clast patches that underlie *Bedform a* show upstream pinch-out of sandstone beds and downstream amalgamation (Fig. 7) indicating multiple flow events formed these patches and the lower sandstone body prior to the initiation of the main bedform. The presence of these mudstone clast patches results in a marked difference in bedform architecture and bed thickness for *Bedform a* compared to *Bedform b* and *c*.

Bed-scale process record - Old Railway section

In the Old Railway section (Fig. 11), erosional bed bases and bed amalgamation are common, particularly where there is depositional thinning of underlying beds, indicating that the 'pinch-and-swell' bedforms present at this section are the result of multiple flow events in contrast to the Doornkloof area. However, bed amalgamation has limited impact on bedform thickness, as thickness increase dominantly occurs downdip of the point of amalgamation and is therefore of a depositional nature. The Old Railway bedforms classify as sediment waves (Wynn & Stow, 2002) with dimensions of 15 to >40 m wavelength (extending outside outcrop limits) and 1-2 m amplitude. However, the maximum bed thicknesses (1-1.5 m) are more limited than at the Doornkloof area (>2.5 m), climbing ripple-laminated facies (F3) is more dominant, and banded facies (F2) are almost absent. The sediment waves have a more uniform facies distribution and there is an absence of internal truncation surfaces (Fig. 11). The dominance of F3 indicates rapid deposition from dilute turbulent flows, which contrasts with the Doornkloof area.

Subcritical sediment waves: comparison with supercritical bedforms

The Doornkloof and Old Railway outcrops are both characterised by composite sediment waves. However, there are distinct differences between both areas. The Old Railway examples exhibit comparatively simple sediment waves, composed of multiple event beds, and dominated by lower flow-regime facies (F3) such as climbing ripple-lamination, accrete downstream, and lack significant internal erosive surfaces. Morphologically, stoss sides can be comparable to or longer than lee sides (Fig. 11). In contrast, the Doornkloof sediment waves were formed as single event beds and are characterized by short stoss sides, long lee sides, and exhibit erosion and more energetic facies (F1, F2, F4), with climbing ripple deposition (F3) becoming more dominant at the top of the beds (Fig. 13A). The Doornkloof waves migrate upstream through erosional truncation and draping at bed swelling locations (up to >10 m; Fig. 9) followed by the development of another bed swell upstream (Fig. 13A). This means that each swell initiates individually, rather than simultaneously as a sinusoidal wave.

The architecture of the Doornkloof sediment waves most closely resembles the smaller-scale type II and type III antidunal bedforms described by Schminke *et al.* (1973). However, these bedform architectures, which are an order of magnitude smaller, are interpreted to migrate through stoss-side deposition by supercritical flows based on the field observations, and have never been produced experimentally. In contrast, Kubo & Nakajima (2002) and Kubo (2004) observed sediment wave architectures with short stoss sides, long lee sides and variable wavelengths, similar to the Doornkloof sediment waves, under subcritical flow conditions in physical and numerical experiments. The depositional patterns of these sediment waves were defined by upstream migration of waveforms by individual growing mounds (Kubo & Nakajima, 2002; Kubo, 2004), and are therefore highly analogous to the observations from the Doornkloof waves.

The nature and variability of small-scale bedform structures (F3) (e.g., Fig. 13A for the Doornkloof waves) provide key indicators of flow type. This facies group consists of climbing ripples, sinusoidal lamination, biconvex ripples, and hummock-like structures, with biconvex ripples sometimes transitioning upwards into the hummocks. Climbing ripples and sinusoidal lamination are indicators of subcritical flow (Allen, 1973; Southard & Boguchwal, 1990), and the biconvex ripples and hummock-like structures have greater affinities with combined-flow ripples and hummocky cross stratification than with antidunes, again suggesting deposition under subcritical flow conditions. In particular, the vertical change from biconvex ripples to hummock-like bedforms observed in the Doornkloof sediment waves is strongly analogous to structures associated with reflected flows in other turbidites (Tinterri, 2011; Tinterri & Muzzi Magalhaes, 2011), rather than deposits associated with supercritical flow conditions. The presence of topography in the form of the large-scale sediment wave may have led to flow reflection (Tinterri, 2011) and deflection as and when the flow waned. Importantly, these subcritical small-scale bedforms are observed over the full length of the sediment waves, both on the stoss- and lee-side, at Doornkloof and the Old Railway (Figs 5, 9 and 11). This indicates subcritical deposition occurred across the entire sediment wave, and that the flow remained subcritical throughout the depositional period over which the decimetre bedforms were formed.

The morphology and architecture of the sediment waves in this study contrast with large supercritical bedforms, such as cyclic steps, since these exhibit short erosional lee-sides and long depositional stoss-sides (Cartigny *et al.*, 2014; Hughes-Clark, 2016), and display upstream sediment wave migration as a sinusoidal wave (Cartigny *et al*. 2014). Additionally, the sediment waves described here are not single bedform structures such as described from supercritical bedforms (e.g., Cartigny *et al*., 2014; Covault *et al*., 2017), but are composed of stacked smaller-scale bedforms. The spatial and temporal extent of subcritical deposits also contrasts strongly with 'supercritical' bedforms where subcritical deposition can be expected only in some or all of the stoss-side, downdip of a hydraulic jump (Vellinga *et al*., 2018). Furthermore, tractional subcritical bedforms are predicted to be limited to the downstream parts of the stoss side in aggradational cyclic steps, or to be mixed-in with supercritical and non-tractional subcritical facies in transportational cyclic steps (Vellinga *et al*., 2018; their Fig. 9). Note that decimeter-scale bedforms themselves could not be modelled in the CFD simulations of Vellinga *et al*. (2018). Lastly, the overall signature of subcritical deposits within dominantly supercritical bedforms was one dominated by amalgamation of concave-up erosional surfaces and low-angle foresets and backsets creating lenticular bodies (Vellinga *et al*., 2018). These bodies scale with the size of the overall bedform, and the backsets show clear downstream fining (Vellinga *et al*., 2018). Again, the sediment waves studied herein show radically different architecture to that formed in cyclic steps, characterised by stacked decimeter-scale bedforms and an absence of large-scale (scaling with the sediment wave) foresets, backsets and lenticular bodies.

In summary, the morphology, architecture, composite nature, and small-scale bedform types, all indicate that the sediment waves were clearly deposited under subcritical conditions. The subcritical nature of these sediment waves, the observation of upstream accretion via deposition on the stoss side, and the associated upstream migration of the crestline, observed at Doornkloof, challenge the assumption that all upstream-orientated expansion of sediment waves is the product of supercritical conditions (Wynn & Stow, 2002; Symons *et al*., 2016). That said, the Doornkloof bedforms appear to have migrated sporadically over short distances (m's to tens of m's) through upstream accretion (Fig. 9B), before undergoing growth of new sediment wave lenses upstream, thus the entire bedform does not continuously migrate as observed in some modern sediment wave examples (e.g., Hughes-

Clark, 2016). The presence of these subcritical sediment waves in the downstream parts of CLTZs also challenges the idea that mid-sized fans, like those in the Karoo, likely exhibit flows close to critical Froude numbers, at and beyond the CLTZ (Hamilton *et al*., 2017), although such conditions are likely in upstream parts of CLTZ where scouring occurs.

Spatio-temporal flow fluctuations

The large-scale erosive truncations, and the wide variability of decimetre-scale bedforms in space and time, observed in the Doornkloof waves indicate marked spatio-temporal flow fluctuations from a single flow event. In contrast, the continuity of facies and absence of significant erosive surfaces suggests that the Old Railway sediment waves were formed by flows with very limited spatio-temporal variation. Here, we focus on these spatio-temporal fluctuations indicated by the Doornkloof waves, and later address the issue of how the different types of sediment waves shown in the Doornkloof and Old Railway outcrops could coexist.

Fluctuations in velocity and concentration can be expected in environments where turbidity currents exit confinement (e.g. Kneller & McCaffrey, 1999, 2003; Ito, 2008; Kane *et al*., 2009; Ponce & Carmona, 2011), and where flows pass over depositional and erosional relief on the seabed (e.g. Groenenberg *et al*., 2010; Eggenhuisen *et al*., 2011). Similar steep internal scour surfaces to those observed in the Doornkloof bedforms were interpreted to be generated by energetic sweeps from a stratified flow (Hiscott, 1994b). Furthermore, a similar depositional history of waxing and waning behaviour within a single flow was inferred from the sediment waves of the Miocene Austral foreland Basin, Argentina (Ponce & Carmona, 2011). However, the depositional model proposed by Ponce & Carmona (2011) assumes each independent lens-shaped geometry is created and reworked simultaneously, and subsequently draped as a result of flow deceleration. The Doornkloof sediment wave architecture cannot be explained by this process as the ‘lenses’ are clearly not disconnected (Figs 5 and 13). The distribution of truncation surfaces within the sediment waves of subunit B2 does however suggest there can be both phases of upstream swell formation as well as upstream migration of the crest line (e.g. *Bedform c* at log 34-35). To explain the large fluctuations in flow concentration and depositional behaviour in CLTZ settings (Fig. 13), a number of factors can be considered. Here, we consider each of these factors in turn, and assess their potential for explaining the development of the sediment waves observed in this study.

Flow splitting in updip channel-levée systems

Waxing and waning flow behaviour can be induced by splitting of the flow in the channel-levée system updip, where the primary 'channelised' flow may reach the sediment wave field earlier than the secondary 'overbank' flow (Peakall *et al*., 2000). However, this would imply significant velocity and concentration differences and therefore significant depositional facies differences between the two stages, which does not fit the observations (Figs 13 and 14A). Furthermore, it would not explain the number of flow fluctuations interpreted within a single flow event bed (Figs 13 and 14A).

Mixed load (sand-clay) bedforms

An alternative explanation for the sediment wave architecture could be that these bedforms formed by flows with sand-clay mixtures. Complicated bedform architectures with both erosional and depositional components have been created experimentally (Baas *et al.*, 2016). However, there are a number of issues with this hypothesis: 1) the bedforms described from the two case studies are one to two orders of magnitude larger than the 'muddy' bedforms described within flume tanks (Baas *et al.*, 2016), and 2) the presence of clean climbing ripple-lamination suggests that at least part of the flow was not clay-rich during deposition (Baas *et al*., 2013; Schindler *et al*., 2015).

Froude number fluctuations

The net-depositional record of waxing and waning flow conditions (Fig. 14A) observed at a single given location within the Doornkloof sediment waves (Fig. 13) could be hypothesised to be a record of temporal fluctuations around the critical Froude number separating sub- and supercritical flow conditions. However, the evidence for subcritical deposition across the full length of the sediment waves, and over the timescale of bedform development, demonstrates that fluctuations around the critical Froude number cannot be directly responsible for the formation of these sediment waves. That said, fluctuations in velocity and capacity within a subcritical flow downstream of a zone of hydraulic jumps may still play a role in controlling the observed sedimentation patterns. Fluctuations of the turbidity current Froude number are expected in areas of abrupt flow expansion such as at the base-of-slope (Garcia, 1993; Wynn *et al*., 2002b). Turbidity currents that undergo rapid transitions from supercritical to subcritical conditions forming a single hydraulic jump, or repeated hydraulic jumps across a CLTZ (Sumner *et al*., 2013; Dorrell *et al*., 2016), have been linked to bedform formation (Vicente Bravo & Robles, 1995; Wynn & Stow, 2002; Wynn *et al*., 2002b; Symons *et al*., 2016), and have been linked to the formation of erosive scours in upstream parts of CLTZs in the Karoo Basin (Hofstra *et al*., 2015). Due to the presence of multiple interacting hydraulic jumps across a CLTZ, Froude number fluctuations around unity may be expected (Sumner *et al*., 2013; Dorrell *et al*., 2016). Such velocity fluctuations would change the capacity of the flow (Fig. 14A), however whether this would translate to periodic changes in sediment concentration is less clear due in part to the lack of concentration measurements from natural and experimental subaqueous hydraulic jumps. That said, in turbidity currents generally, there is a close coupling between velocity and concentration changes (Felix *et al*., 2005). Fluctuating velocities, and potentially concentration, related to variations in Froude numbers around critical may enable complicated and variable bedform architectures to be formed.

The 'hose effect'

A spatial control in flow character could also be invoked to explain the development of sediment waves, based on flow-deposit interactions and the momentum of the flow core (Fig. 14B). As a turbidity current exits channel confinement it does not directly lose its momentum (e.g. Choi & Garcia, 2001). The flow core may shift around during bedform aggradation due to interactions with depositional and erosional relief around the channel-mouth. Most studies on flow-deposit interactions focus on temporal changes in flow conditions (e.g. Kneller & McCaffrey, 2003; Groenenberg *et al.,* 2010), but rarely consider lateral changes within a single turbidity current (Hiscott, 1994a). A single location within a sediment wave field may receive periods of high and low energy linked to the lateral shifting of the flow core, where the energetic flow core can be linked to periods of erosion and/or high concentration flow deposition, and the flow margin to deposition from the less energetic and dilute parts of the flow. In this scenario, the upstream-orientated truncation surfaces are the result of the interaction of the flow core with its self-produced obstacle (Fig. 14B), linked to the inability to sustain the compensation process over time. Upstream fluctuations in Froude number, related to an area of scour formation and hydraulic jumps, would result in longitudinal waxing and waning flow behaviour downstream and could explain the combination of both erosion and high concentration flow deposition of the flow core.

The compensational effects will form a stratigraphic record of fluctuating energy levels (Figs 13A and 14A). The lateral flow movement may explain deviation in palaeoflow direction between intra-bed ripple-laminated intervals compared to sediment wave bed tops, observed within the Doornkloof subunit B2 sediment waves (Figs 4A, 6F, 13 and 14), as it could represent (partial) flow deflection affected by the evolving sediment wave morphology. Similar behaviour within a single unconfined flow has been invoked in basin-floor settings of the Cloridorme Formation (Parkash, 1970; Parkash & Middleton, 1970) and at levée settings of the Amazon Channel (Hiscott *et al*., 1997). The 'hose effect' would result in a composite depositional record as the core of the flow sporadically moves laterally, repeatedly superimposing high energy conditions onto lower energy conditions, therefore explaining the inconsistency in sediment wave wavelengths. With this spatial process, the locus of deposition will move laterally whilst the waning flow can lead to deposition progressively migrating upstream. The hose effect may explain how sediment waves are able to build upstream accreting geobodies without being deposited under supercritical conditions. The mechanism also provides an explanation for the range and spatial variability of the observed small-scale bedform structures (F3), and for the similarities with small-scale bedforms interpreted to have been formed by turbidity currents interacting with topography (Tinterri, 2011; Tinterri & Muzzi Magalhaes, 2011). As the flow migrates laterally, flows will interact at an angle with the growing sediment wave, thus encouraging interaction of incident and reflected flow.

As noted earlier, there is strong field-evidence (Parkash, 1970; Parkash & Middleton, 1970; Hiscott *et al*., 1997) for the 'hose effect' mechanism. However, the hose effect has not been experimentally or numerically modelled, which reflects the ubiquity of bedform experiments in two-dimensional flumes, and a paucity of three-dimensional flow effects on bedform development.

Spatio-temporal flow fluctuations - summary

In summary, the combination of waxing and waning flow behaviour in the subcritical flow core, downstream of a zone of hydraulic jumps (Dorrell *et al*., 2016), as well as spatial compensational processes (hose effect) are invoked as the most probable mechanisms to explain the complicated architecture and facies patterns of the Doornkloof sediment waves.

Spatial variations within a sediment wave field

As noted earlier, there are major differences between the sediment waves at the Old Railway outcrop with a low degree of spatial and temporal variability, and the high spatio-temporal variability observed in the Doornkloof sediment waves. Here, we will attempt to explain such variation between sediment waves in the same system. One potential mechanism is the character of the feeder channel, including factors such as channel dimensions and magnitude of the incoming flows. However, previous studies (Brunt *et al*., 2013) suggest that the dimensions of feeder channels within the Unit B base-of-slope system were similar, implying that the character of sediment waves is unrelated to variations in feeder channel character.

Alternatively, the differences between the Doornkloof and Old Railway areas may be related to their position relative to the mouth of the feeder channel. A dominance of lower flow-regime facies (F3) such as climbing ripple-lamination is commonly associated with overbank or off-axis environments (e.g. Kane & Hodgson, 2011; Brunt *et al*., 2013; Rotzien *et al*., 2014). As the Old Railway is characterised by such facies, it could represent a fringe position through a sediment wave field (Fig. 15). In contrast, the Doornkloof section is characterized by erosion and more energetic facies (F1, F2, F4), suggesting it was situated in a more axial position in the sediment wave field (Fig. 15A). Furthermore, within the Doornkloof area, climbing ripple deposition (F3) becomes more dominant at the top of the beds, likely reflecting progressive decrease in flow velocity and concentration (Figs 5, 8 and 9B). These spatial and temporal variations can be integrated with the hypothesised lateral shifting of the flow core (the hose effect). The hose effect is likely to have more influence on deposits within axial parts of the channel-mouth, such as within the Doornkloof area, where the flow is most powerful. In contrast, the lateral fringes of the channel-mouth are most likely subject to deposition from flow margins (Fig. 15B), such as at the Old Railway section. This results in more steady flow conditions and relatively uniform deposition of facies and explains the difference in characteristics between the Old Railway sediment waves, which are dominated by F3 facies and shows little evidence of erosion, and the Doornkloof sediment waves, which are dominated by F1 and F2 facies with substantial evidence of erosion.

The differences in the expression of the Unit B sediment waves suggest that the stratigraphic record of CLTZ environments exhibit substantial spatial variability. The process model shows that initial sediment wave architecture can involve both upstream orientated accretion (Doornkloof area), and downstream orientated accretion (Old Railway section), depending on the position with respect to the channel mouth. Despite the lack of 3D control on morphology, we predict that this variance in depositional behaviour between axial and fringe areas will have influence on planform crest morphology and will lead to the crest curvatures, which are commonly observed within the modern seafloor (e.g. Wynn *et al*., 2002b). Similar observations on the importance of spatial variation have been made for the erosional bedform area (Fig. 15) of channel lobe transition zones (Hofstra *et al*., 2015).

Preservation of sediment waves in channel lobe transition zones

Two questions that remain unanswered are: 1) what conditions promoted stratigraphic preservation of the sediment waves in the examples herein, and 2) how likely is preservation of sediment waves in the stratigraphic record of channel lobe transition zones? Here, we interpret that the preservation of the sediment waves in the two field areas is related to the strongly aggradational character of subunits B1 and B2. This is also evident from the lobe deposits downdip that show strong aggradation and limited progradation (Fig. 3; Brunt *et al*., 2013), in comparison to lobe deposits elsewhere in the Karoo Basin (e.g., Hodgson *et al*., 2006; van der Merwe *et al*., 2014). Furthermore, subunit B1 is abruptly overlain by a regional mudstone aiding preservation, whereas subunit B2 is overlain by thick levée successions (subunit B3), marking the progradation of the slope system across the CLTZ (Brunt *et al*., 2013). This scenario has similarities to that proposed by Pemberton *et al*. (2016) who suggested that preservation of scours in a CLTZ was linked to a rapidly prograding slope system.

For sediment waves in CLTZ settings in general, there are several scenarios that can be proposed to facilitate their preservation. During system initiation at the start of a waxing-to-waning sediment supply cycle, possibly driven by a relative sea-level fall and initial slope incision, the position of the CLTZ on the base-of-slope might be relatively stable as slope conduits evolve prior to slope progradation. The stratigraphic record of the resulting deposits is likely limited in thickness, and probably preferentially associated with scour-fills (e.g., Pemberton *et al*., 2016). The position of the CLTZ could be fixed through physiographic features, such as a tectonic or diapiric break-in-slope, which would aid the stratigraphic preservation of the CLTZ. Several studies have shown that when submarine channel-levee systems avulse they do not return to their original route (e.g. Armitage *et* *al*., 2012; Ortiz-Karpf *et al*., 2015; Morris *et al*., 2016), which would help to preserve sediment waves in an abandoned CLTZ. The stratigraphic evidence for this control would be in the sediment waves abruptly overlain by mudstone or thin-bedded successions indicative of overbank deposition. Finally, the preservation potential of sediment waves in CLTZs will be higher at the point of maximum regression/progradation of the system (Hodgson *et al*., 2016). Similar arguments were applied to the preservation of scour-fills in CLTZ by Hofstra *et al*. (2015).

In summary, we hypothesise that preservation of sediment waves may require i) updip avulsion, ii) represent the point of maximum system progradation, or iii) form during a period of relative spatial stability, followed by system progradation. Subsequent rapid progradation of a slope system is then important for long-term preservation, though an off-axis location relative to large-scale slope channels is critical in order to avoid cannibalisation of the CLTZ deposits (e.g., Hofstra *et al*., 2015). Such propagation of channel-levée systems (e.g. Hodgson *et al.,* 2016), suggests that the preservation potential of sediment waves in axial positions, for example the interpreted position of the Doornkloof section, is lower than sediment wave deposits in fringe positions, such as the interpreted position of the Old Railway section (Fig. 15A).

CONCLUSIONS

Detailed morphologies, architectures and facies of fine-sand grained sediment waves are reported from an ancient channel-lobe transition zone. The sediment waves are constructed from banded and planar-laminated sandstones, as well as from progressive aggradation of a range of small-scale bedforms, including climbing ripples, sinusoidal lamination, biconvex ripples, and hummocky-like structures, interpreted as the products of subcritical deposition, with periods of flow reflection and deflection forming the biconvex ripples and hummocks. Morphologically, the sediment waves exhibit long-lee sides, and short erosively-cut stoss sides, and show upstream accretion over short distances (m’s to tens of m’s), punctuated by the upstream development of new sediment wave lenses. Consequently, the observations from these exhumed deposits challenge some current models of sediment wave development, which suggest that entire sediment waves continuously migrate upstream under supercritical conditions. In particular, the outcrops demonstrate that the formation of sediment waves in an upstream direction, as well as upstream migration of crestlines, is not solely the product of supercritical flows, but can also occur in subcritical conditions. The progressive development of the sediment waves is argued to be the product of lateral migration of the expanding flow across the channel-lobe transition zone, potentially coupled to fluctuations in velocity and flow capacity related to upstream hydraulic jumps. Variations in sediment waves, from more complex forms with multiple erosive surfaces and complex internal facies, to simple accretionary forms with abundant climbing ripples, is linked to position across the channel-lobe transition zone, from axial to lateral fringes respectively. The preservation potential of sediment waves in CLTZs into the stratigraphic record is low due to subsequent system progradation and erosion. However, preservation is higher where there is updip avulsion and abandonment of a CLTZ, in off axis areas where sediment waves might be overlain by overbank sediments, and / or at the point of maximum system progradation.

ACKNOWLEDGEMENTS

This work forms part of the results of the LOBE 2 joint industry consortium research project. We are grateful for the financial support from: Anadarko, Bayerngas Norge, BG Group, BHP Billiton, BP, Chevron, Dong Energy, E.ON, GDF Suez, Maersk Oil, Marathon Oil, Petrobras, Shell, Statoil, Total, VNG Norge, and Woodside. We are grateful to Matthieu Cartigny, Brian Romans and an anonymous reviewer for the constructive reviews and for the input of Associate Editor Jaco Baas, which greatly improved this manuscript. We also acknowledge the landowners from the Laingsburg area for access to their land. Finally, Renée de Bruijn, Nienke Lips and Yvonne Spychala are thanked for their assistance in the field.

REFERENCES

Alexander, J., Bridge, J.S., Cheel, R.J. and **Leclair, S.F.** (2001) Bedforms and associated sedimentary structures formed under supercritical water flows over aggrading sand beds. *Sedimentology,* **48**, 133-152.

Allen, J.R.L. (1973) A classification of climbing-ripple cross-lamination. *Journal of the Geological Society of London*, **129**, 537-541.

Allen, J.R.L. (1984) Parallel lamination developed from upper-stage plane beds: a model based on the larger coherent structures of the turbulent boundary layer. *Sedimentary Geology,* **39**, 227-242.

Armitage, D.A., McHargue, T., Fildani, A. and **Graham, S.A.** (2012) Postavulsion channel evolution: Niger Delta continental slope. *AAPG Bulletin*, **96***,* 823-843.

Baas, J.H. and **de Koning, H.** (1995) Washed-out ripples: Their equilibrium dimensions, migration rate, and relation to suspended-sediment concentration in very fine sand. *Journal of Sedimentary Research*, **65**, 431-435.

Baas, J.H., Davies, A.G. and **Malarkey, J.** (2013) Bedform development in mixed sand-mud: The contrasting role of cohesive forces in flow and bed. *Geomorphology*, **182**, 19-32.

Baas, J.H., Best, J.L. and **Peakall, J.** (2016) Predicting bedforms and primary current stratification in cohesive mixtures of mud and sand. *Journal of the Geological Society,* 1**73**, 12-45.

Best, J. and **Bridge, J.** (1992) The morphology and dynamics of low amplitude bedwaves upon upper stage plane beds and the preservation of planar laminae. *Sedimentology,* **39**, 737-752.

Bouma, A.H. and **Boerma, J.A.K.** (1968) Vertical disturbances in piston cores. *Marine Geology*, **6**, 231-241.

Brunt, R.L., Hodgson, D.M., Flint, S.S., Pringle, J.K., Di Celma, C., Prélat, A. and **Grecula, M.** (2013) Confined to unconfined: Anatomy of a base of slope succession, Karoo Basin, South Africa. *Marine and Petroleum Geology*, **41**, 206-221.

Campion, K.T., Dixon, B.T. and **Scott, E.D.** (2011) Sediment waves and depositional implications for fine-grained rocks in the Cerro Toro Formation (Upper Cretaceous), Silla Syncline, Chile. *Marine and Petroleum Geology,* **28**, 761-784.

Cartigny, M.J., Eggenhuisen, J.T., Hansen, E.W. and **Postma, G.** (2013) Concentration-dependent flow stratification in experimental high-density turbidity currents and their relevance to turbidite facies models. *Journal of Sedimentary Research*, **83**, 1047-1065.

Cartigny, M.J.B., Ventra, D., Postma, G. and **Van Den Berg, J.H.** (2014) Morphodynamics and sedimentary structures of bedforms under supercritical-flow conditions: New insights from flume experiments. *Sedimentology*, **61**, 712-748.

Choi, S.U. and **Garcia, M.H.** (2001) Spreading of gravity plumes on an incline. *Coastal Engineering Journal,* **43**, 221-237.

Covault, J.A., Kostic, S., Paull, C.K., Sylvester, Z. and **Fildani, A.** (2017) Cyclic steps and related supercritical bedforms: Building blocks of deep-water depositional systems, western North America. *Marine Geology*, **393**, 4-20, doi:10.1016/j.margeo.2016.12.009

Damuth, J.E. (1979) Migrating sediment waves created by turbidite currents in northern South China Basin. *Geology*, **7**, 520-523.

Dorrell, R.M., Peakall, J., Sumner, E.J., Parsons, D.R., Darby, S.E., Wynn, R.B., Özsoy, E. and **Tezcan, D.** (2016) Flow dynamics and mixing processes in hydraulic jump arrays: Implications for channel-lobe transition zones. *Marine Geology*, **381**, 181-193.

Dumas, S. and **Arnott, R.W.C.** (2006) Origin of hummocky and swaley cross-stratification— The controlling influence of unidirectional current strength and aggradation rate. *Geology*, **34**, 1073-1076.

Dumas, S., Arnott, R.W.C. and **Southard, J.B.** (2005) Experiments on oscillatory-flow and combined-flow bed forms: Implications for interpreting parts of the shallow-marine sedimentary record. *Journal of Sedimentary Research*, **75**, 501-513.

Eggenhuisen, J.T., McCaffrey, W.D., Haughton, P.D. and **Butler, R.W.** (2011) Shallow erosion beneath turbidity currents and its impact on the architectural development of turbidite sheet systems. *Sedimentology*, **58**, 936-959.

Fedele, J.J., Hoyal, D., Barnaal, Z., Tulenko, J. and **Awatt, S.** (2017) Bedforms created by gravity flows. In: Budd, D.A., Hajek, E.A. and Purkis, S.J. (Eds) *Autogenic Dynamics and Self-organization in Sedimentary Systems*. SEPM Special Publication 106, 95-121.

Felix, M., Sturton, S. and **Peakall, J.** (2005) Combined measurements of velocity and concentration in experimental turbidity currents. *Sedimentary Geology*, **179**, 31-47.

Flint, S.S., Hodgson, D.M., Sprague, A., Brunt, R.L., Van Der Merwe, W.C., Figueiredo, J., Prélat, A., Box, D., Di Celma, C. and **Kavanagh, J.P.** (2011) Depositional architecture and sequence stratigraphy of the Karoo basin floor to shelf edge succession, Laingsburg depocentre, South Africa. *Marine and Petroleum Geology,* **28**, 658-674.

Garcia, M.H. (1993) Hydraulic jumps in sediment-driven bottom currents. *Journal of Hydraulic Engineering,* **119**, 1094-1117.

Garcia, M.H. (2008) Sedimentation Engineering: Process, Measurements, Modeling and Practice. American Society of Civil Engineers, Reston, Virginia.

Grecula, M., Flint, S.S., Wickens, H.DeV. and **Johnson, S.D.** (2003) Upward-thickening patterns and lateral continuity of Permian sand-rich turbidite channel fills, Laingsburg Karoo, South Africa. *Sedimentology,* **50**, 831-853.

Groenenberg, R.M., Hodgson, D.M., Prélat, A., Luthi, S.M. and **Flint, S.S.** (2010) Flow-deposit interaction in submarine lobes: insights from outcrop observations and realizations of a process-based numerical model. *Journal of Sedimentary Research*, **80**, 252-267.

Hamilton, P., Gaillot, G., Strom, K., Fedele, J. and **Hoyal, D.** (2017) Linking hydraulic properties in supercritical submarine distributary channels to depositional lobe geometry. *Journal of Sedimentary Research*, **87**, 935-950.

Harms, J.C. (1969) Hydraulic significance of some sand ripples. *Geological Society of America Bulletin*, **80**, 363-396.

Harms, J.C., Southard, J.B., Spearing, D.R. and **Walker, R.G.** (1975) *Depositional environments as interpreted from primary sedimentary structures and stratification sequences*. Society for Sedimentary Geology (SEPM) Short Course 2, pp. 161.

Haughton, P., Davis, C., McCaffrey, W. and **Barker, S.** (2009) Hybrid sediment gravity flow deposits-classification, origin and significance. *Marine and Petroleum Geology*, **26**, 1900-1918.

Heiniö, P. and **Davies R.J.** (2009) Trails of depressions and sediment waves along submarine channels on the continental margin of Espirito Santo Basin, Brazil. *Geological Society of America Bulletin*, **121**, 698-711.

Hiscott, R.N. (1994a) Loss of capacity, not competence, as the fundamental process governing deposition from turbidity currents. *Journal of Sedimentary Research*, **64**, 209-214.

Hiscott, R.N. (1994b) Traction-carpet stratification in turbidites-fact or fiction? *Journal of Sedimentary Research,* **64**, 204-208.

Hiscott, R.N., Hall, F.R., and **Pirmez, C.** (1997) Turbidity-current overspill from the Amazon Channel: texture of the silt/sand load, paleoflow from anisotropy of magnetic susceptibility, and implications for flow processes. In: *Proceedings of the Ocean Drilling Program, Scientific Results* (Eds. Flood, R.D., Piper, D.J.W., Klaus, A. and Peterson, I.C.), **155**, 53-78.

Hodgson, D.M., Flint, S.S., Hodgetts, D., Drinkwater, N.J., Johannessen, E.P. and **Luthi, S.M.** (2006) Stratigraphic evolution of fine-grained submarine fan systems, Tanqua depocenter, Karoo Basin, South Africa. *Journal of Sedimentary Research*, **76**, 20-40.

Hodgson, D.M., Di Celma, C.N., Brunt, R.L. and **Flint, S.S.** (2011) Submarine slope degradation and aggradation and the stratigraphic evolution of channel-levee systems. *Journal of the Geological Society*, **168**, 625-628.

Hodgson, D.M., Kane, I.A., Flint, S.S., Brunt, R.L. and **Ortiz-Karpf, A.** (2016). Time-transgressive confinement on the slope and the progradation of basin-floor fans: Implications for the sequence stratigraphy of deep-water deposits. *Journal of Sedimentary Research*, **86**, 73-86.

Hofstra, M. (2016) The Stratigraphic Record of Submarine Channel-lobe Transition Zones. Unpublished PhD thesis, University of Leeds, Leeds, 331p.

Hofstra, M., Hodgson, D.M., Peakall, J. and **Flint, S.S.** (2015) Giant scour-fills in ancient channel-lobe transition zones: Formative processes and depositional architecture. *Sedimentary Geology,* **329**, 98-114.

Howe, J.A. (1996) Turbidite and contourite sediment waves in the northern Rockall Trough, North Atlantic Ocean. *Sedimentology,* **43**, 219-234.

Hughes Clarke, J.E. (2016) First wide-angle view of channelized turbidity currents links migrating cyclic steps to flow characteristics. *Nature Communications,* 7:11896, doi: 10.1038/ncomms11896.

Ito, M. (2008) Downfan transformation from turbidity currents to debris flows at a channel-to-lobe transitional zone: the lower Pleistocene Otadai Formation, Boso Peninsula, Japan. *Journal of Sedimentary Research,* **78**, 668-682.

Ito, M. (2010) Are coarse-grained sediment waves formed as downstream-migrating antidunes? Insight from an early Pleistocene submarine canyon on the Boso Peninsula, Japan. *Sedimentary Geology,* **226**, 1-8.

Ito, M. and **Saito, T.** (2006) Gravel waves in an ancient canyon: Analogous features and formative processes of coarse-grained bedforms in a submarine-fan system, the lower Pleistocene of the Boso Peninsula, Japan. *Journal of Sedimentary Research*, **76**, 1274-1283.

Ito, M., Ishikawa, K. and **Nishida, N.** (2014) Distinctive erosional and depositional structures formed at a canyon mouth: A lower Pleistocene deep-water succession in the Kasuza forearc basin on the Boso Peninsula, Japan. *Sedimentology*, **61**, 2042-2062.

Jobe, Z.R., Lowe, D.R. and **Morris, W.R.** (2012) Climbing-ripple successions in turbidite systems: depositional environments, sedimentation rates and accumulation times. *Sedimentology*, **59**, 867-898.

Johansson, M. and **Stow, D.A.V.** (1995) A classification scheme for shale clasts in deep water sandstones. In: Hartley, A.J. and Prosser, D.J. (eds.) *Characterization of Deep Marine Clastic Systems*, Geological Society Special Publication 94, 221-241.

Jopling, A.V. and **Walker, R.G.** (1968) Morphology and origin of ripple-drift cross-lamination, with examples from the Pleistocene of Massachusetts. *Journal of Sedimentary Research,* **38**, 971-984.

Kane, I.A. and **Hodgson, D.M.** (2011) Sedimentological criteria to differentiate submarine channel levee subenvironments: exhumed examples from the Rosario Fm. (Upper Cretaceous) of Baja California, Mexico, and the Fort Brown Fm. (Permian), Karoo basin, S. Africa. *Marine and Petroleum Geology*, **28**, 807-823.

Kane, I.A., McCaffrey, W.D. and **Martinsen, O.J.** (2009) Allogenic vs. autogenic controls on megaflute formation. *Journal of Sedimentary Research*, **79**, 643-651.

Kennedy, J.F. (1969) The formation of sediment ripples, dunes and antidunes. *Annual Review of Fluid Mechanics*, **1**, 147-168.

Kidd, R.B., Lucchi, R.G., Gee, M. and **Woodside, J.M.** (1998) Sedimentary processes in the Stromboli Canyon and Marsili Basin, SE Tyrrhenian Sea: results from side-scan sonar surveys. *Geo-Marine Letters*, **18**, 146-154.

Kneller, B. (1995) Beyond the turbidite paradigm: physical models for deposition of turbidites and their implications for reservoir prediction. In: *Characterization of Deep Marine Clastic Systems* (Eds. Hartley, A.J. and Prosser, D.J.) *Geol. Soc. London, Spec. Publ*., **94**, 31-49.

Kneller, B.C. and **Branney, M.J.** (1995) Sustained high-density turbidity currents and the deposition of thick massive sands. *Sedimentology*, **42**, 607-616.

Kneller, B.C. and **McCaffrey, W.D.** (1999) Depositional effects of flow nonuniformity and stratification within turbidity currents approaching a bounding slope: deflection, reflection, and facies variation. *Journal of Sedimentary Research*, **69**, 980-991.

Kneller, B.C. and **McCaffrey, W.D.** (2003) The interpretation of vertical sequences in turbidite beds: the influence of longitudinal flow structure. *Journal of Sedimentary Research*, **73**, 706-713.

Kubo, Y. (2004) Experimental and numerical study of topographic effects on deposition from two-dimensional, particulate-driven density currents. *Sedimentary Geology*, **164**, 311-326.

Kubo, Y. and **Nakajima, T.** (2002) Laboratory experiments and numerical simulation of sediment-wave formation by turbidity currents. *Marine Geology,* **192**, 105-121.

Lonsdale, P. and **Hollister, C.D.** (1979) Near-bottom traverse of Rockall Trough-Hydrographic and geological inferences. *Oceanologica Acta,* **2**, 91-105.

Lowe, D.R. (1982) Sediment gravity flows: II Depositional models with special reference to the deposits of high-density turbidity currents. *Journal of Sedimentary Research*, **52**, 279-297.

Macdonald, H.A., Wynn, R.B., Huvenne, V.A., Peakall, J., Masson, D.G., Weaver, P.P. and **McPhail, S.D.** (2011) New insights into the morphology, fill, and remarkable longevity (>0.2 m.y.) of modern deep-water erosional scours along the northeast Atlantic margin. *Geosphere*, **7**, 845-867.

Malinverno, A., Ryan, W.B., Auffret, G. and **Pautot, G.** (1988) Sonar images of the path of recent failure events on the continental margin off Nice, France. In*: Sedimentological Consequences of Convulsive Geologic Events,* (Ed. Clifton, H.E.), *Geological Society of America Special Paper,* **229**, 59-76.

McHugh, C.M. and **Ryan, W.B.** (2000) Sedimentary features associated with channel overbank flow: examples from the Monterey Fan. *Marine Geology*, **163**, 199-215.

Migeon, S., Savoye, B., Zanella, E., Mulder, T., Faugères, J.C. and **Weber, O.** (2001) Detailed seismic-reflection and sedimentary study of turbidite waves on the Var Sedimentary Ridge (SE France): significance for sediment transport and deposition and for the mechanisms of sediment-wave construction. *Marine and Petroleum Geology*, **18**, 179-208.

Morris, S.A., Kenyon, N.H., Limonov, A.F. and **Alexander, J.** (1998) Downstream changes of large-scale bedforms in turbidites around the Valencia channel mouth, north-west Mediterranean: implications for palaeoflow reconstruction. *Sedimentology,* **45**, 365-377.

Morris, E.A., Hodgson, D.M., Brunt, R.L. and **Flint, S.S.** (2014) Origin, evolution and anatomy of silt-prone submarine external levées. *Sedimentology*, **61**, 1734-1763.

Morris, E.A., Hodgson, D.M., Flint, S., Brunt, R.L., Luthi, S.M. and **Kolenberg, Y**. (2016) Integrating outcrop and subsurface data to assess the temporal evolution of a submarine channel–levee system. *AAPG Bulletin*, **100**, 1663-1691.

Mulder, T. and **Alexander, J.** (2001) The physical character of subaqueous sedimentary density flows and their deposits. *Sedimentology*, **48**, 269-299.

Mukti, M.M.R. and **Ito, M.** (2010) Discovery of outcrop-scale fine-grained sediment waves in the lower Halang Formation, an upper Miocene submarine-fan succession in West Java. *Sedimentary Geology*, **231**, 55-62.

Mutti, E. and **Normark, W.R.** (1987) Comparing examples of modern and ancient turbidite systems: problems and concepts. In: *Marine Clastic Sedimentology: Concepts and Case Studies* (Eds. Leggett, J.K. and Zuffa, G.G.) *Graham and Trotman, Oxford,* pp. 1-38.

Mutti, E. and **Normark, W.R.** (1991) An integrated approach to the study of turbidite systems. In: *Seismic Facies and Sedimentary Processes of Submarine Fans and Turbidite Systems* (Eds. Weimer, P. and Link, M.H.) *Springer, New York*, pp. 75-106.

Nakajima, T., Satoh, M. and **Okamura, Y.** (1998) Channel-levee complexes, terminal deep-sea fan and sediment wave fields associated with the Toyama Deep-Sea Channel system in the Japan Sea. *Marine Geology*, **147**, 25-41.

Normark, W.R. and **Dickson, F.H.** (1976) Sublacustrine fan morphology in Lake Superior. *AAPG Bulletin*, 60, 1021-1036.

Normark, W.R. and **Piper, D.J.W.** (1991) Initiation processes and flow evolution of turbidity currents: Implications for the depositional record. In: *From Shoreline to Abyss: Contributions in Marine Geology in Honor of Francis Parker Shepard* (Ed. Osborne, R.H.), *SEPM Special Publication*, **46**, 207-230.

Normark W.R., Hess, G.R., Stow, D.A.V. and **Bowen, A.J.** (1980) Sediment waves on the Monterey Fan levee: a preliminary physical interpretation. *Marine Geology*, **37**, 1-18.

Normark, W.R., Piper, D.J., Posamentier, H. Pirmez, C. and **Migeon, S.** (2002) Variability in form and growth of sediment waves on turbidite channel levees. *Marine Geology*, **192**, 23-58.

Ortiz-Karpf, A., Hodgson, D.M. and **McCaffrey, W.D.** (2015) The role of mass-transport complexes in controlling channel avulsion and the subsequent sediment dispersal patterns on an active margin: the Magdalena Fan, offshore Colombia. *Marine and Petroleum Geology*, **64**, 58-75.

Palanques, A., Kenyon, N.H., Alonso, B. and **Limonov, A.** (1995) Erosional and depositional patterns in the Valencia mouth: An example of a modern channel-lobe transition zone channel. *Marine Geophysical Researches*, **17**, 503-517.

Parkash, B. (1970) Downcurrent changes in sedimentary structures in Ordovician turbidite greywackes. *Journal of Sedimentary Research*, **40**, 572-590.

Parkash, B. and **Middleton, G.V.** (1970) Downcurrent textural changes in Ordovician turbidite greywackes. *Sedimentology*, **14**, 259-293.

Peakall, J., McCaffrey, W.D. and **Kneller, B.C.** (2000) A process model for the evolution, morphology, and architecture of sinuous submarine channels. *Journal of Sedimentary Research*, **70**, 434–448.

Pemberton, E.A.L., Hubbard, S.M., Fildani, A., Romans, B. and **Stright, L.** (2016) The stratigraphic expression of decreasing confinement along a deep-water sediment routing system: Outcrop example from southern Chile. *Geosphere*, **12**, 114-134.

Piper, D.J.W. and **Kontopoulos, N.** (1994) Bed forms in submarine channels: comparison of ancient examples from Greece with studies of Recent turbidite systems. *Journal of Sedimentary Research,* **64**, 247-252.

Piper, D.J.W., Shor, A.N., Farre, J.A., O'Connell, S. and **Jacobi, R.** (1985) Sediment slides and turbidity currents on the Laurentian Fan: Sidescan sonar investigations near the epicenter of the 1929 Grand Banks earthquake. *Geology*, **13**, 538-541.

Ponce, J.J. and **Carmona, N.** (2011) Coarse-grained sediment waves in hyperpycnal clinoform systems, Miocene of the Austral foreland basin, Argentina. *Geology*, **39**, 763-766.

Postma, G., Kleverlaan, K. and **Cartigny, M.J.B.** (2014) Recognition of cyclic steps in sandy and gravelly turbidite sequences and consequences for the Bouma facies. *Sedimentology*, **61**, 2268-2290.

Praeg, D.B. and **Schafer, C.T.** (1989) Seabed features of the Labrador slope and rise near 55° N revealed by SEAMARC I sidescan sonar imagery. *Atlantic Geoscience Centre, Bedford Institute of Oceanography.*

Prave, A.R. and **Duke, W.L.** (1990) Small-scale hummocky cross-stratification in turbidites: a form of antidune stratification? *Sedimentology*, **37**, 531-539.

Prélat, A. and **Hodgson, D.M.** (2013) The full range of turbidite bed thickness patterns in submarine lobes: controls and implications. *Journal of the Geological Society,* **170**, 209-214.

Prélat, A., Hodgson D.M. and **Flint, S.S.** (2009) Evolution, architecture and hierarchy of distributary deep-water deposits: a high-resolution outcrop investigation from the Permian Karoo Basin, South Africa. *Sedimentology*, **56**, 2132-2154.

Prélat, A., Covault J.A., Hodgson D.M., Fildani, A. and **Flint, S.S.** (2010) Intrinsic controls on the range of volumes, morphologies, and dimensions of submarine lobes. *Sedimentary Geology*, **232**, 66-76.

Pringle, J.K., Brunt, R.L., Hodgson, D.M. and **Flint, S.S.** (2010) Capturing stratigraphic and sedimentological complexity from submarine channel complex outcrops to digital 3D models, Karoo Basin, South Africa. *Petroleum Geoscience*, **16**, 307-330.

Raudkivi, A.J. (1998) *Loose Boundary Hydraulics*. A.A. Balkema, Rotterdam, The Netherlands, pp 260.

Rotzien, J.R., Lowe, D.R., King, P.R. and **Browne, G.H.** (2014) Stratigraphic architecture and evolution of a deep-water slope channel-levee and overbank apron: The Upper Miocene Upper Mount Messenger Formation, Taranaki Basin. *Marine and Petroleum Geology*, **52**, 22-41.

Schindler, R.J., Parsons, D.R., Ye, L., Hope, J.A., Baas, J.H., Peakall, J., Manning, A.J., Aspden, R.J., Malarkey, J., Simmons, S., Paterson, D.M., Lichtman, I.D., Davies, A.G., Thorne, P.D. and **Bass, S.J.**

(2015) Sticky stuff: Redefining bedform prediction in modern and ancient environments. *Geology*, **43**, 399-402.

Schminke, H.U., Fisher, R.V. and **Waters, A.C.** (1973) Antidune and chute and pool structures in the base surge deposits of the Laacher See area, Germany. *Sedimentology*, **20**, 553-574.

Sixsmith, P., Flint, S.S., Wickens, H.D. and **Johnson, S.** (2004) Anatomy and stratigraphic development of a basin floor turbidite system in the Laingsburg Formation, main Karoo Basin, South Africa. *Journal of Sedimentary Research*, **74**, 239-254.

Skipper, K., (1971) Antidune cross-stratification in a turbidite sequence, Cloridorme Formation, Gaspé, Quebec. *Sedimentology*, **17**, 51-68.

Sohn, Y.K. (1997) On traction-carpet sedimentation. *Journal of Sedimentary Research*, **67**, 502-509.

Southard, J.B. (1991) Experimental determination of bed-form stability. *Annual Review of Earth and Planetary Sciences*, **19**, 423-455.

Southard, J.B. and **Boguchwal, L.A.** (1990) Bed configurations in steady unidirectional water flows. Part 2. Synthesis of flume data. *Journal of Sedimentary Research*, **60**, 658-679.

Stow, D.A. and **Johansson, M.** (2000) Deep-water massive sands: nature, origin and hydrocarbon implications. *Marine and Petroleum Geology*, **17**, 145-174.

Stevenson, C.J., Jackson, C.A-L., Hodgson, D.M., Hubbard, S.M. and **Eggenhuisen, J.T.** (2015) Deep-water sediment bypass. *Journal of Sedimentary Research*, **85**, 1058-1081.

Sumner, E.J., Amy, L.A. and **Talling, P.J.** (2008) Deposit structure and processes of sand deposition from decelerating sediment suspensions. *Journal of Sedimentary Research*, **78**, 529-547.

Sumner, E.J., Peakall, J., Parsons, D.R., Wynn, R.B., Darby, S.E., Dorrell, R.M., McPhail, S.D., Perrett, J., Webb, A. and **White, D.** (2013) First direct measurements of hydraulic jumps in an active submarine density current. *Geophysical Research Letters*, **40**, 5904-5908.

Symons, W.O., Sumner, E.J., Talling, P.J., Cartigny, M.J. and **Clare, M.A.** (2016) Large-scale sediment waves and scours on the modern seafloor and their implications for the prevalence of supercritical flows. *Marine Geology*, **371**, 130-148.

Talling, P.J., Masson, D.G., Sumner, E.J. and **Malgesini, G**. (2012) Subaqueous sediment density flows: Depositional processes and deposit types. *Sedimentology*, **59**, 1937-2003.

Tinterri, R. (2011). Combined flow sedimentary structures and the genetic link between sigmoidal and hummocky cross-stratification. *GeoActa (Bologna)*, **10**, 1-43.

Tinterri, R. and **Muzzi Magalhaes, P.** (2011) Synsedimentary structural control on foredeep turbidites: An example from Miocene Marnoso-arenacea Formation, Northern Apennines, Italy. *Marine and Petroleum Geology*, **28**, 629-657.

Tinterri, R. and **Tagliaferri, A.** (2015) The syntectonic evolution of foredeep turbidites related to basin segmentation: Facies response to the increase in tectonic confinement (Marnoso-arenacea Formation, Miocene, Northern Apennines, Italy). *Marine and Petroleum Geology*, **67**, 81-110.

Van der Mark, C.F., Blom, A. and **Hulscher, S.J.M.H.** (2008) Quantification of variability in bedform geometry. *Journal of Geophysical Research: Earth Surface*, **113**, F03020, doi:10.1029/ 2007JF000940.

Van Der Merwe, W.C., Hodgson, D.M., Brunt, R.L. and **Flint, S.S.** (2014) Depositional architecture of sand-attached and sand-detached channel-lobe transition zones on an exhumed stepped slope mapped over a 2500 km^2 area. *Geosphere,* **10**, 1076-1093.

Vellinga, A.J., Cartigny, M.J.B., Eggenhuisen, J.T. and **Hansen, E.W.M.** (2018) Morphodynamics and depositional signature of low-aggradation cyclic steps: New insights from a depth resolved model. *Sedimentology*, **65**, 540-560.

Vicente Bravo, J.V. and **Robles, S.** (1995) Large-scale mesotopographic bedforms from the Albian Black Flysch, northern Spain: characterization, setting and comparison with recent analogues. In: *Atlas of Deep Water Environments; Architectural Style in Turbidite Systems* (Eds. Pickering, K.T., Hiscott, R.N., Kenyon, N.H., Ricci-Lucchi, F. and Smith, R.D.A.), *Chapman and Hall, London,* pp. 216-226.

Wickens H.DeV. (1994) Basin floor fan building turbidites of the southwestern Karoo Basin, Permian Ecca Group, South Africa*. PhD-Thesis. University of Port Elizabeth*.

Winn, R.D. and **Dott, R.H.** (1977) Large-scale traction-produced structures in deep-water fan-channel conglomerates in southern Chile. *Geology*, **5**, 41-44.

Wynn, R.B. and **Stow, D.A.** (2002) Classification and characterisation of deep-water sediment waves. *Marine Geology,* **192**, 7-22.

Wynn, R.B., Kenyon, N.H., Masson, D.G., Stow D.A. and **Weaver, P.P.** (2002a) Characterization and recognition of deep-water channel-lobe transition zones. *AAPG Bulletin*, **86**, 1441-1462.

Wynn, R.B., Piper, D.J.W. and **Gee, M.J.R.** (2002b) Generation and migration of coarse-grained sediment waves in turbidity current channels and channel-lobe transition zones. *Marine Geology*, **192**, 59-78.

Yokokawa, M., Matsuda, F. and **Endo, N.** (1995) Sand particle movement on migrating combined-flow ripples. *Journal of Sedimentary Research*, **A65**, 40-44.

Zecchin, M., Caffau, M., Di Stefano, A., Maniscalco, R., Lenaz, D., Civile, D., Muto, F. and **Crantelli, S.** (2013) The Messinian succession of the Crotone Basin (southern Italy) II: Facies architecture and stratal surfaces across the Miocene-Pliocene boundary. *Marine and Petroleum Geology*, **48**, 474-492.

FIGURE CAPTIONS

Figure 1. Sediment wave dimensions (crest height *versus* wavelength) from modern and ancient systems grouped on the basis of type of dataset (A), setting (B) and grain size (C). Data taken from Normark & Dickson (1976); Winn & Dott (1977); Damuth (1979); Lonsdale & Hollister (1979); Piper *et al.* (1985); Malinverno *et al.* (1988); Praeg & Schafer (1989); Piper & Kontopoulos (1994); Vicente Bravo & Robles (1995); Howe (1996); Kidd *et al.* (1998); Morris *et al.* (1998); Nakajima *et al.* (1998); McHugh & Ryan (2000); Migeon *et al.* (2001); Wynn *et al.* (2002a,b); Normark *et al.* (2002); Ito & Saito (2006); Heinïo & Davies (2009); Ito (2010); Mukti & Ito (2010); Campion *et al.* (2011); Ponce & Carmona (2011); Ito *et al.* (2014); Morris *et al.* (2014); Postma *et al.* (2014). Note that a lack of sand-prone sediment waves in modern examples can be ascribed to difficulties in retrieving piston cores within such sediments (e.g. Bouma & Boerma, 1968). The raw data are available as supplementary material to this manuscript.

Figure 2. (A) Location map of the Laingsburg depocentre within the Western Cape. The transparent overlay with black lining indicates the total exposed area of Unit B. Important outcrop areas are highlighted, including the sections studied in this paper: Doornkloof and Old Railway; white diamonds indicate locations discussed in Brunt *et al*. (2013). (B) Zoomed-in map of the Doornkloof section including palaeocurrent distributions, sub-divided into subunit B1 and subunit B2. The outcrop outlines are indicated by solid lines. Red line indicates Section I (Figure 5), blue line on DK-unit B2 represents Section II (Figure 9). (C) Zoomed-in map of the Old Railway section including palaeocurrent distributions.

Figure 3. (A) Simplified stratigraphic column of the deep-water stratigraphy within the Laingsburg depocentre, based on Flint *et al.* (2011). (B-C) Palaeogeographic reconstruction of subunit B2 (B) and subunit B1 (C) based on the regional study of Brunt *et al.* (2013). The two outcrop locations discussed in this paper are indicated by the diamonds.

Figure 4. Examples of Internal bed structure and facies changes within subunit B2 (Doornkloof), with one example from *Bedform c* (A) and two from *Bedform b* (B and C) (see Fig. 9B for locations). All these examples show vertical internal facies changes, which include planar-lamination, wavy-lamination/banding and ripple-lamination.

Figure 5. Complete stratigraphic panel of the Doornkloof section showing the subdivision of Unit B, the location of the two detailed sedimentary sections (I, II), and the position of the DK01 core. The thin siltstone interval (TSI; Brunt *et al*., 2013) between the AB interfan and subunit B1 has been used as a stratigraphic datum. The middle correlation panel shows section I of subunit B1; the position of *Bedform a* and the palaeoflow patterns have been indicated, as well as the location of the correlation panel in Figure 8. The bottom correlation panel shows the detailed facies distribution within *Bedform a* and its internal truncation surfaces. Outcrop photograph locations shown in Figure 6 (A-D) and Figure 7 have been indicated.

Figure 6. Representative outcrop photographs from Section I and II and descriptive DK01 core log of subunit B1, with (A) *Bedform a* with ripple-top morphology on top of a local mudstone clast conglomerate deposit; (B) Eastward-orientated internal truncation surface (dotted line) in banded division within *Bedform a*; (C) Mudstone clast conglomerate layer below *Bedform a*; (D) Mudstone clast-rich banded section of *Bedform a*; (E) Westward-orientated internal truncation surface (dotted line) with climbing ripple-laminated facies within *Bedform a*; (F) Climbing ripple-lamination in between banded sandstone and sigmoidal lamination, as part of *Bedform b*; (G) Lower section of westward orientated truncation surface in *Bedform b;* (H) Upper section of westward orientated truncation surface in *Bedform b;* (I) Banded sandstone division in *Bedform b*; (J) West-facing truncation surface in *Bedform c*. See Figure 5 and Figure 9B for locations. Interpreted position of *Bedform a* is indicated (by an asterisk) within the DK01 core log.

Figure 7. Mudstone clast conglomerate patch at the bottom of *Bedform a*, with clean true-scale photopanel (top) and interpreted vertically exaggerated (Ve = 1.8) photopanel (bottom). It shows a

basal erosion surface overlying thin-bedded sandstones, multiple ‘floating’ sandstone patches, upstream orientated pinch-out and downstream orientated amalgamation. Location of photograph is shown in the lowest panel of Figure 5.

Figure 8. Facies correlation panel of local sandstone swell in subunit B1. *Bedform a* is located at the base of the package. Top panel shows its location within subunit B1. See middle panel of Figure 5 for more detailed facies correlation panel of the complete subunit B1, log locations, and lower panel of Figure 5 for symbol explanations.

Figure 9. (A) Panoramic view of the base of subunit B2 at the DK-section. The outlines of *Bedform b* and *c* are indicated with white lines. Numbers indicate the position of sedimentary logs. (B) Facies correlation of the II-section with *Bedform b* and *c*. The top panel shows the thickness variability of these beds and the surrounding stratigraphy, comprised of structured sandstones (ripple- or planar-laminated); the lower panel shows the internal facies distribution of *Bedform b* and *c*. Rose diagrams show palaeoflow measurements around Section II. Internal truncation surfaces and location of the facies photos shown in Figure 4 and Figure 6 (F-J) have been indicated. See Figure 2B and Figure 5 for location of section II and for meaning of log symbols.

Figure 10. Bedset architecture within the main subunit B2 outcrop face in the Doornkloof area. Bounding surfaces have been defined based on successive bed pinch-out with multiple (3-4) downstream-orientated stacked and weakly amalgamated bedforms.

Figure 11. Subunit B2 within the Old Railway area. A- Facies correlation panels of the section with bedform distribution (top) and facies distribution (bottom). B- Zoomed-in facies correlation panel of most eastern section with C – mudstone clasts within a climbing-ripple laminated bed, indicating sediment overpassing, and D – bed splitting indicating erosion and amalgamation. See Figure 2 for location and lowest panel in Figure 5 for meaning of log symbols. Location of Figure 12 is indicated.

Figure 12. Sketch of bed showing transient pinch-out to a thin siltstone bed (see Figure 11B for location), with (A1) pinch-out to siltstone, and (A2) local scouring of bed top.

Figure 13. (A) Idealised model to illustrate the variation in sedimentary structure within sediment wave swells in the Doornkloof area. (B) Interpretation of changes in depositional behaviour through time, linked to the observed internal facies changes in (A). T1-T7 refer to successive time periods, and show the evolution of the sediment waves, and what this means in terms of flow conditions over time. F1 consists of structureless sands.

Figure 14. (A) Process explanation of the upstream-orientated accretion process, linked to flow capacity changes over time. Flow capacity may be linked to temporal variations in velocity from upstream hydraulic jumps, and/or to the lateral migration of the flow, shown in part B. (B) Illustration of the inferred spatial contribution (hose effect) during formation of the sediment waves. Lateral migration of the flow core during a single event is linked to capacity changes at a single location, as well as the formation of new swells upstream. The steps are interlinked between A and B; ‘x’ marks the same location throughout. Step 5 represents another phase of erosion, and thus a return to step 2.

Figure 15. (A) Spatial division within a channel-lobe transition zone between a depositional bedform area (DB) and an erosional bedform area (EB) following Wynn *et al*. (2002a). Differences in sediment wave deposit facies and architecture are explained by spatial differences between the axis and fringe areas of the deposition-dominated fields (DB) of a CLTZ. (B) Sketch model showing how the ‘hose effect’ within an active flow will dominantly influence sediment wave development in axial areas.

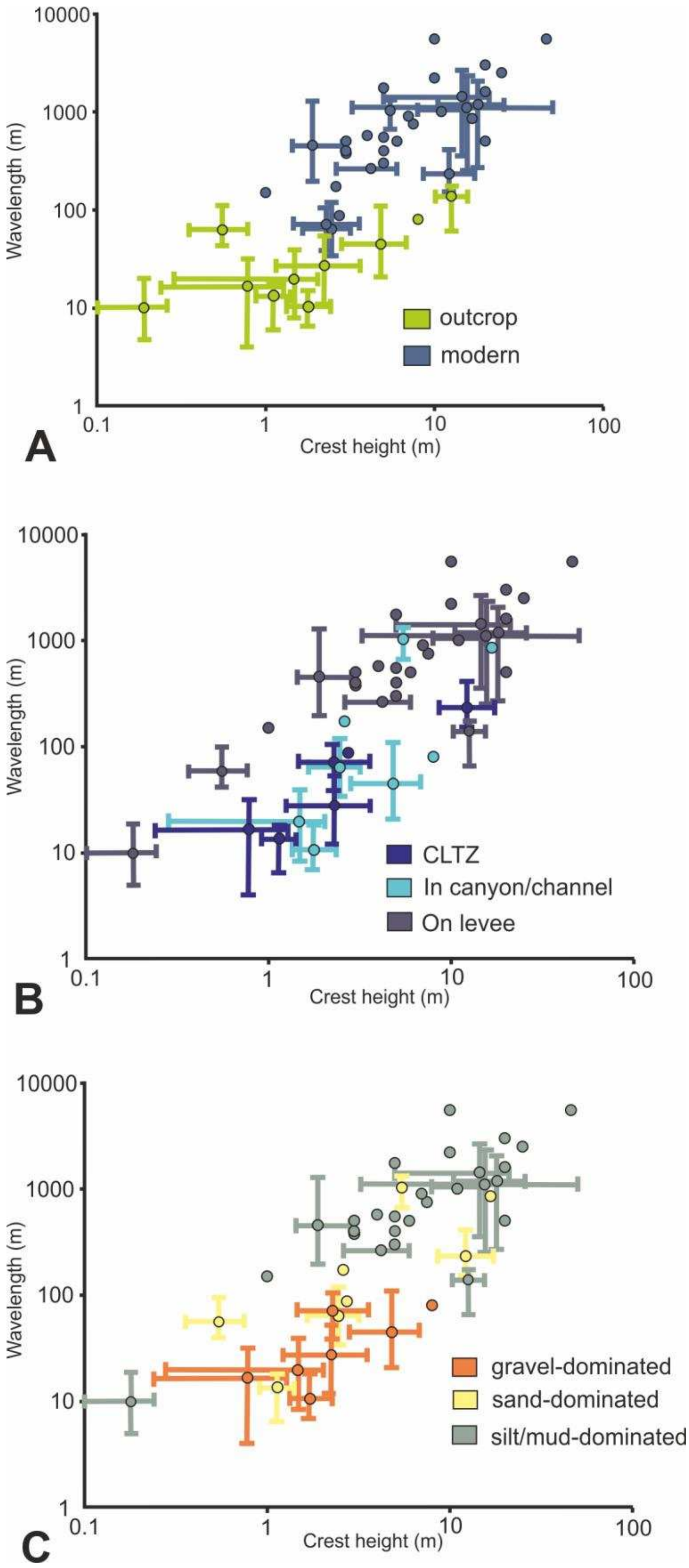
10000
1000
100
10
1
Wavelength (m)
0.1
1
10
100
Crest height (m)
outcrop
modern
A
10000
1000
100
10
1
Wavelength (m)
0.1
1
10
100
Crest height (m)
CLTZ
In canyon/channel
On levee
B
10000
1000
100
10
1
Wavelength (m)
0.1
1
10
100
Crest height (m)
gravel-dominated
sand-dominated
silt/mud-dominated
C

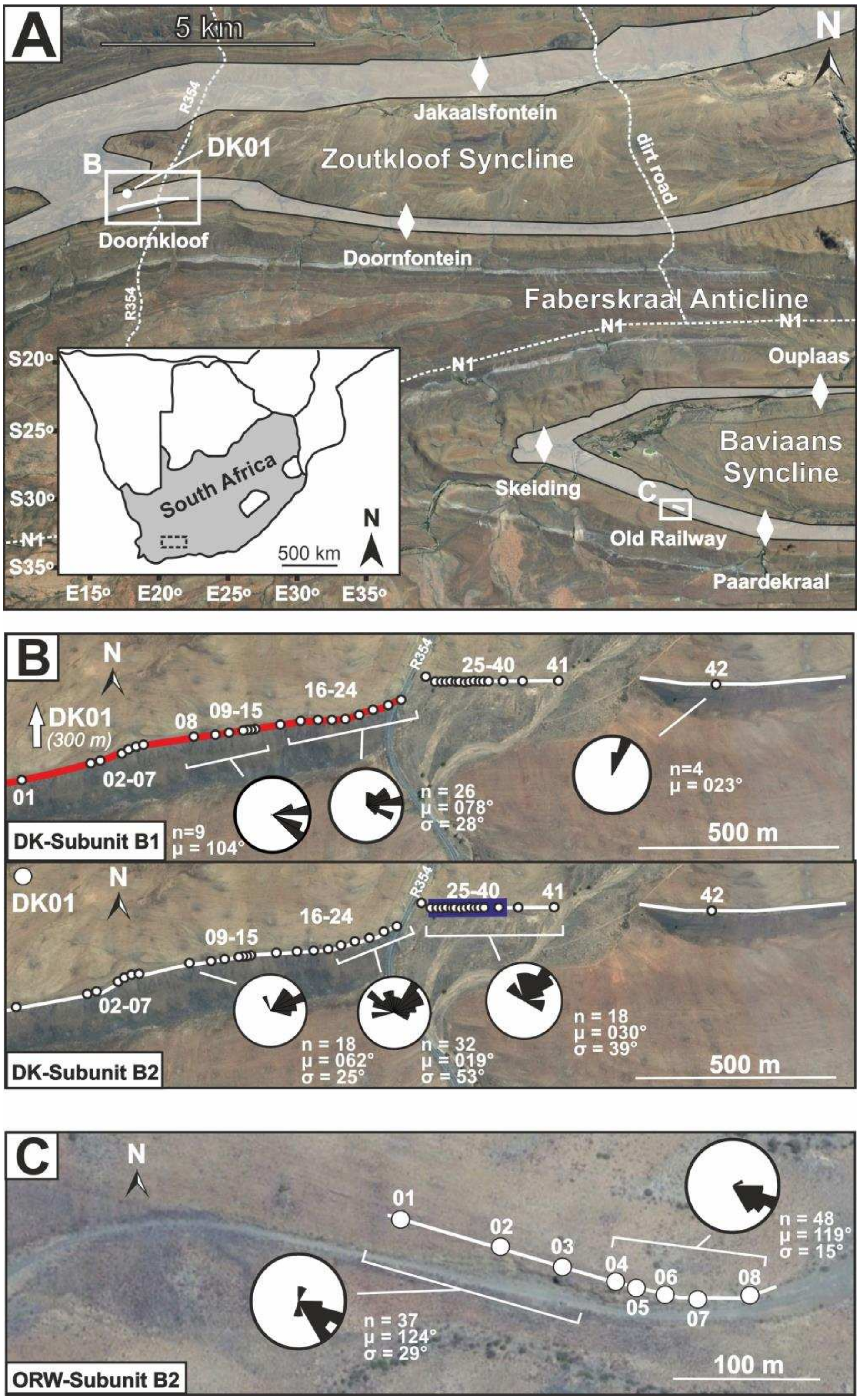
A
5 km
N
R354
Jakaalsfontein
DK01
Zoutkloof Syncline
dirt road
B
Doornkloof
Doornfontein
Faberskraal Anticline
N1
Ouplaas
Baviaans
Syncline
Skeiding
C
Old Railway
Paardekraal
S20°
S25°
S30°
S35°
South Africa
500 km
E15°
E20°
E25°
E30°
E35°
B
DK01
(300 m)
01
02-07
08
09-15
16-24
25-40
41
42
n=9
μ = 104°
n = 26
μ = 078°
σ = 28°
n=4
μ = 023°
500 m
DK-Subunit B1
n = 18
μ = 062°
σ = 25°
n = 32
μ = 019°
σ = 53°
n = 18
μ = 030°
σ = 39°
DK-Subunit B2
C
01
02
03
04
05
06
07
08
n = 48
μ = 119°
σ = 15°
n = 37
μ = 124°
σ = 29°
100 m
ORW-Subunit B2

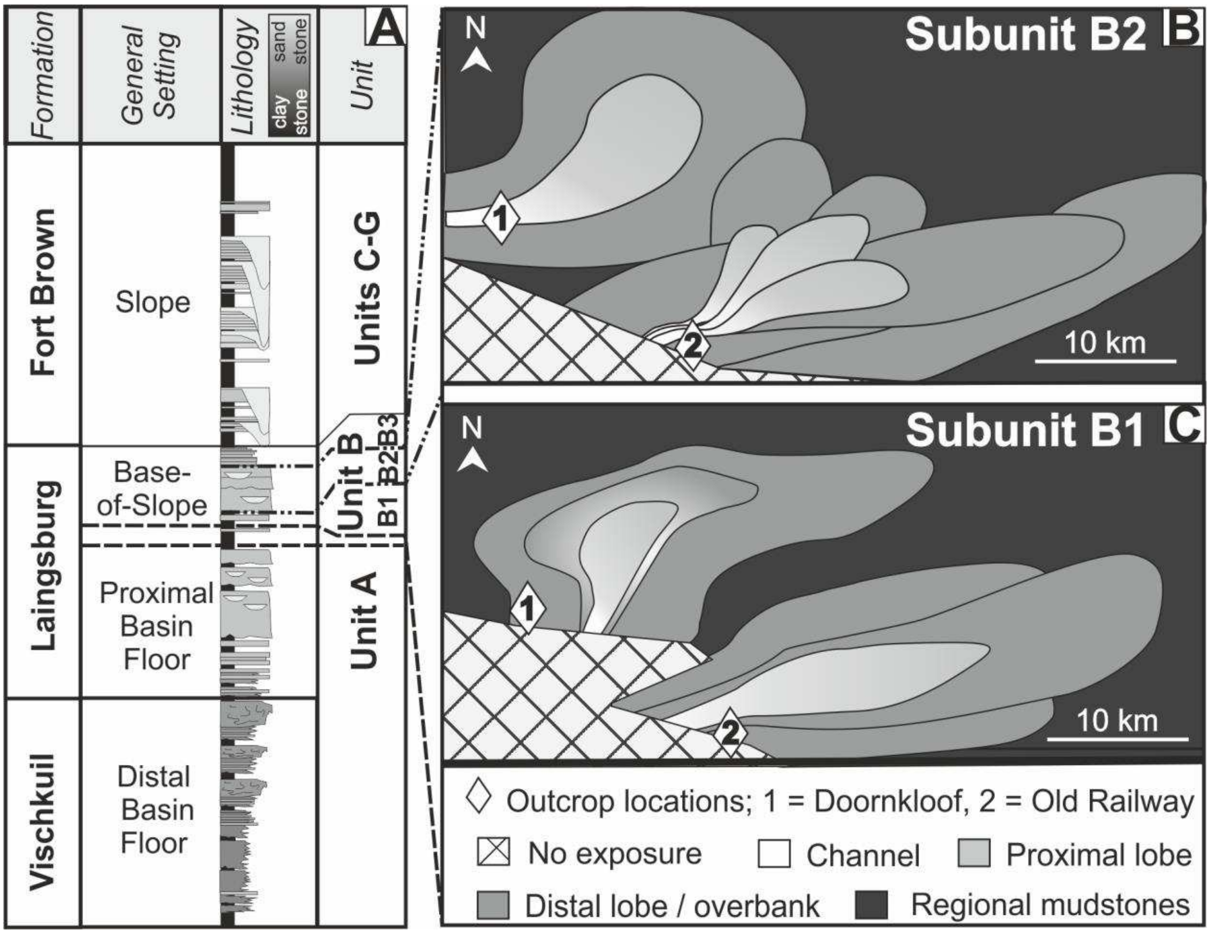
A
Formation
General Setting
Lithology
clay stone
sand stone
Unit
Fort Brown
Slope
Units C-G
Laingsburg
Base-of-Slope
Unit B
B1
B2
B3
Proximal Basin Floor
Unit A
Vischkuil
Distal Basin Floor
Subunit B2
B
N
1
2
10 km
Subunit B1
C
N
1
2
10 km
Outcrop locations; 1 = Doornkloof, 2 = Old Railway
No exposure
Channel
Proximal lobe
Distal lobe / overbank
Regional mudstones

1205

1206

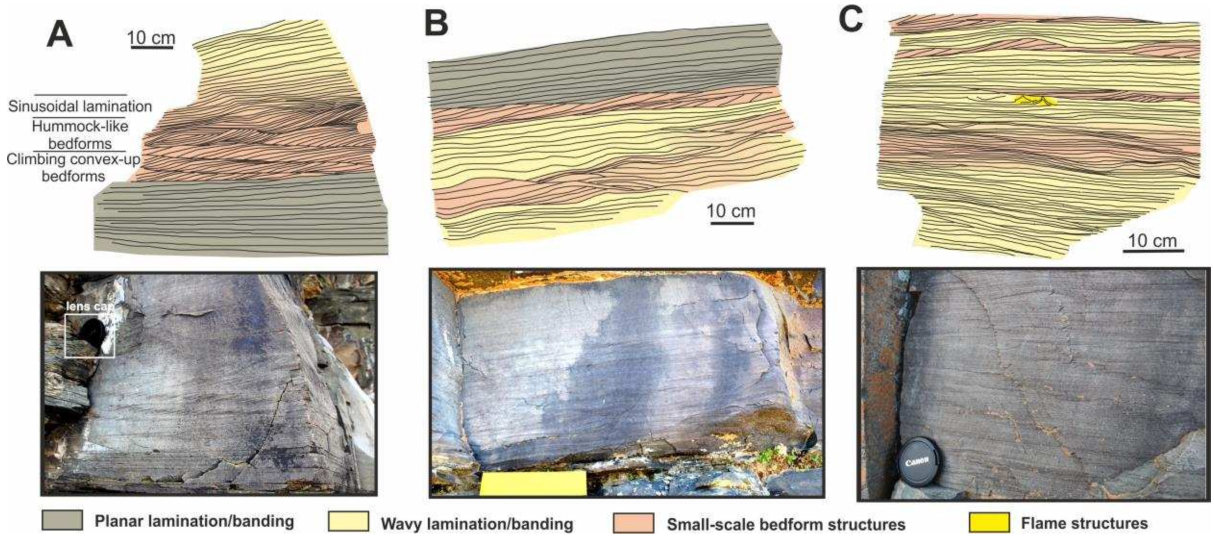
A
10 cm
Sinusoidal lamination
Hummock-like bedforms
Climbing convex-up bedforms
B
10 cm
C
10 cm
lens cap
Planar lamination/banding
Wavy lamination/banding
Small-scale bedform structures
Flame structures

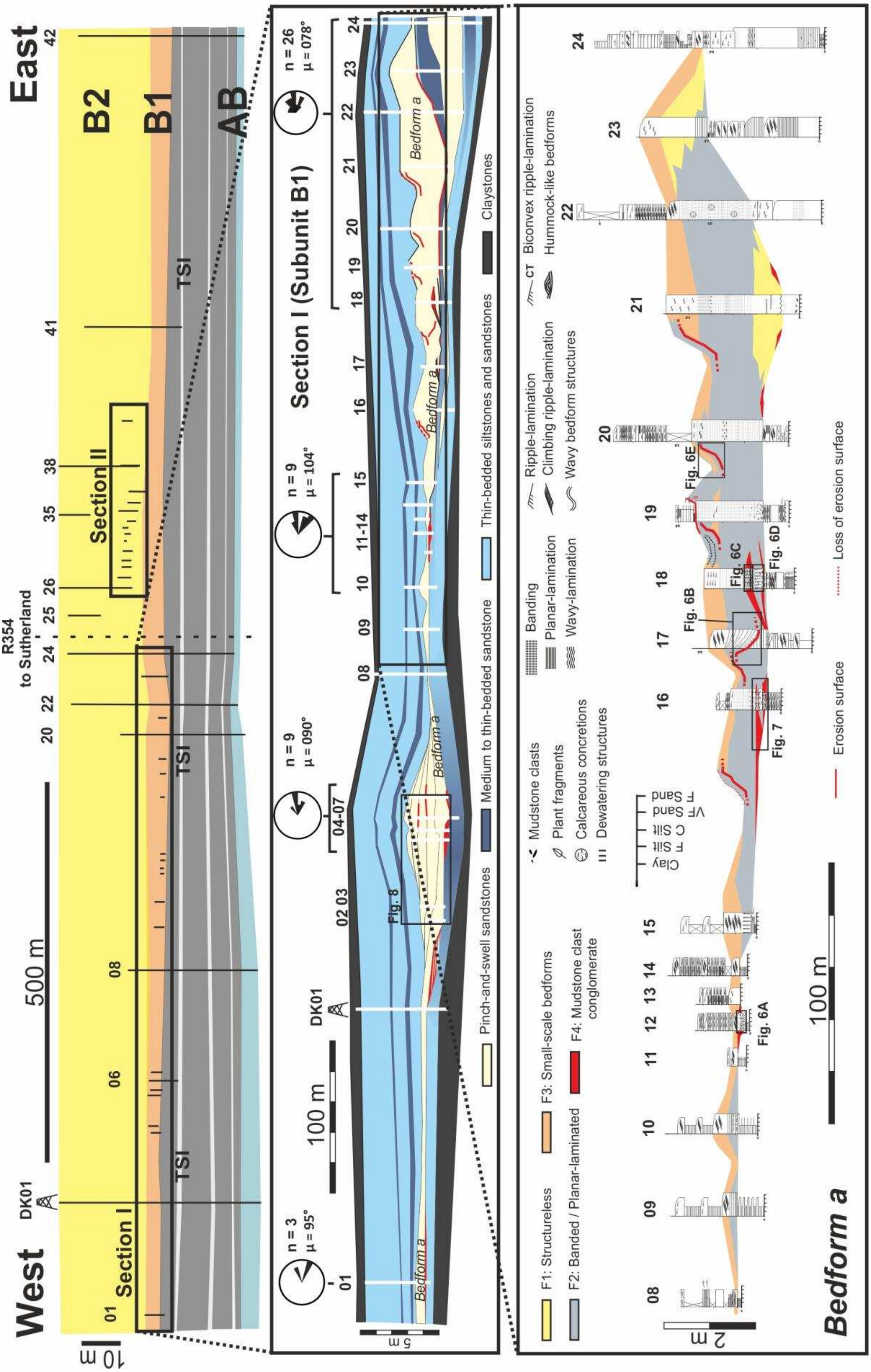

West
East
B2
B1
AB
TSI
Section I
Section II
R354 to Sutherland
DK01
500 m
10 m
Section I (Subunit B1)
Bedform a
n = 3
μ = 95°
n = 9
μ = 090°
n = 9
μ = 104°
n = 26
μ = 078°
Fig. 8
100 m
5 m
Pinch-and-swell sandstones
Medium to thin-bedded sandstone
Thin-bedded siltstones and sandstones
Claystones
F1: Structureless
F2: Banded / Planar-laminated
F3: Small-scale bedforms
F4: Mudstone clast conglomerate
Mudstone clasts
Plant fragments
Calcareous concretions
Dewatering structures
Banding
Planar-lamination
Wavy-lamination
Ripple-lamination
Climbing ripple-lamination
Wavy bedform structures
Biconvex ripple-lamination
Hummock-like bedforms
Erosion surface
Loss of erosion surface
Clay
F Silt
C Silt
VF Sand
F Sand
2 m
Fig. 6A
Fig. 7
Fig. 6B
Fig. 6C
Fig. 6D
Fig. 6E

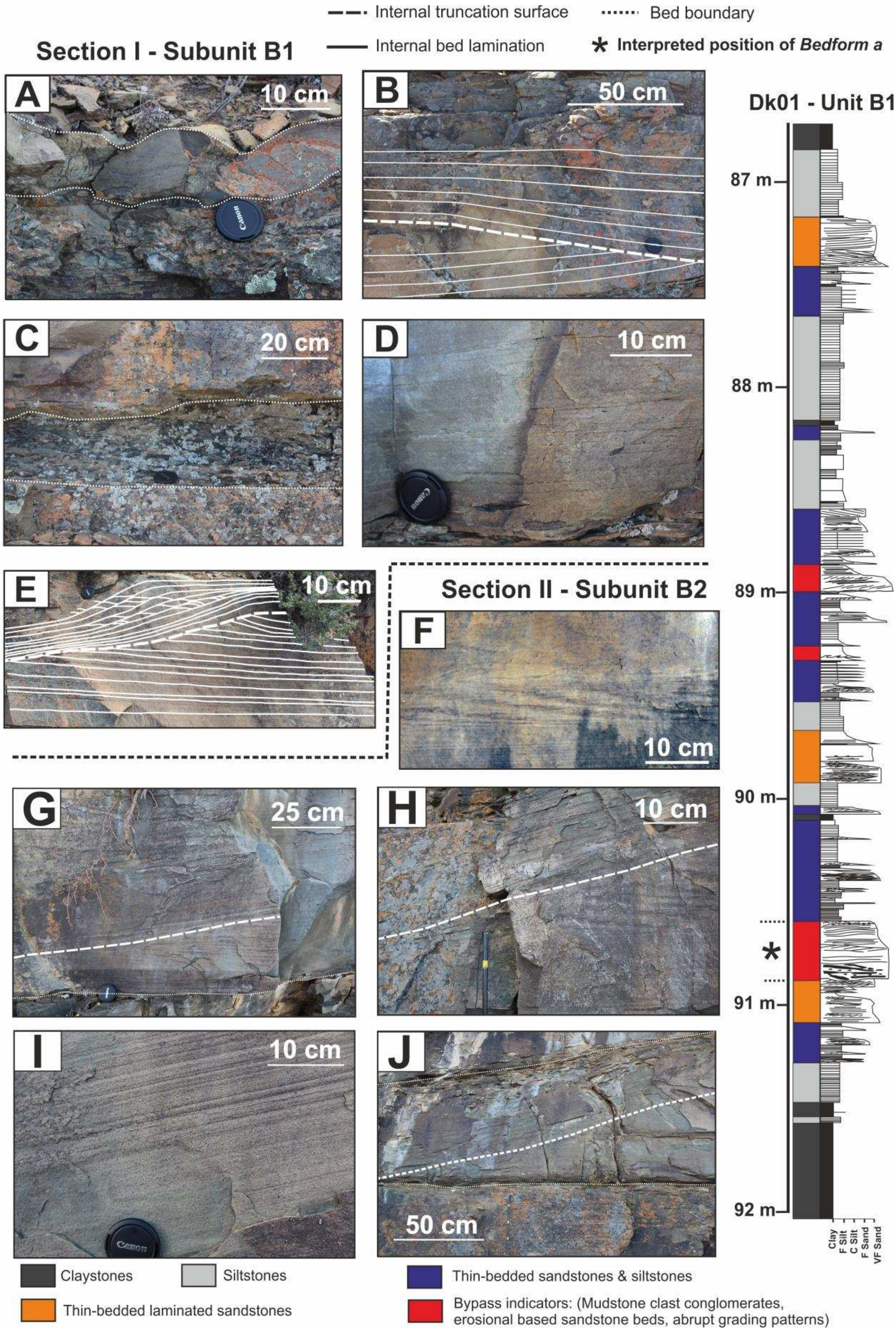

Internal truncation surface
Bed boundary
Internal bed lamination
* Interpreted position of *Bedform a*
Section I - Subunit B1
A
10 cm
B
50 cm
C
20 cm
D
10 cm
E
10 cm
Section II - Subunit B2
F
10 cm
G
25 cm
H
10 cm
I
10 cm
J
50 cm
Dk01 - Unit B1
87 m
88 m
89 m
90 m
91 m
92 m
Clay
F Silt
C Silt
F Sand
VF Sand
Claystones
Siltstones
Thin-bedded sandstones & siltstones
Thin-bedded laminated sandstones
Bypass indicators: (Mudstone clast conglomerates, erosional based sandstone beds, abrupt grading patterns)

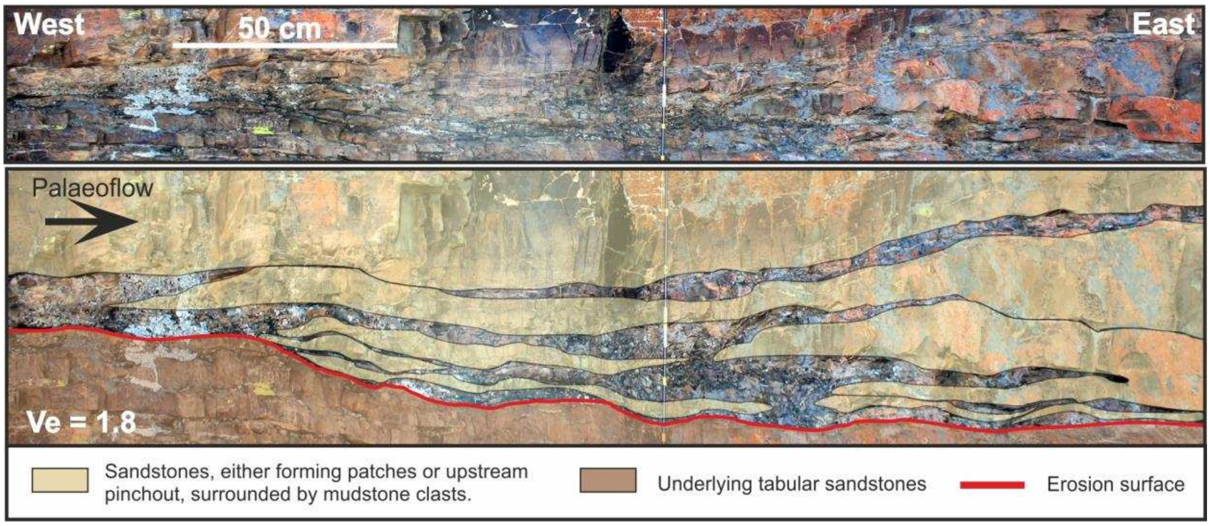
West
50 cm
East
Palaeoflow
Ve = 1.8
Sandstones, either forming patches or upstream pinchout, surrounded by mudstone clasts.
Underlying tabular sandstones
Erosion surface

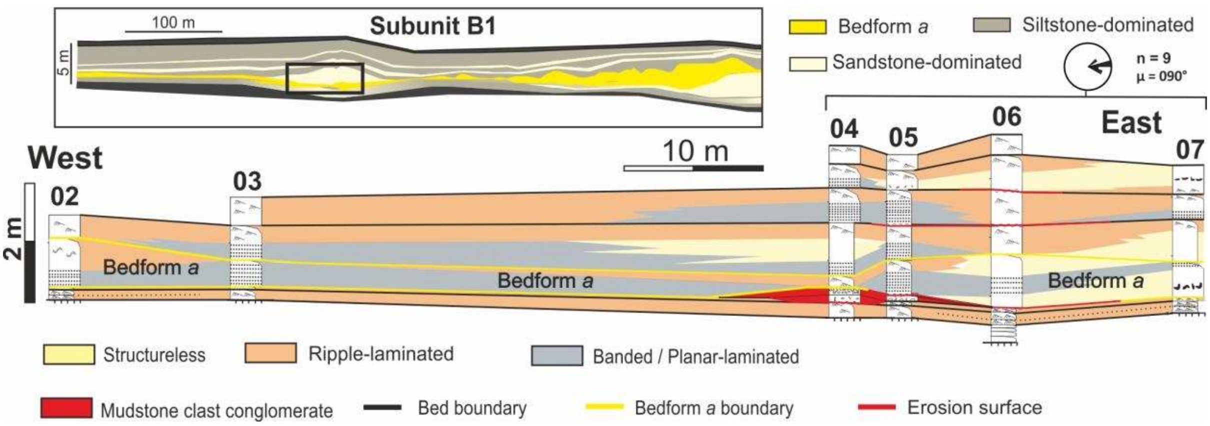

Subunit B1
100 m
5 m
Bedform a
Siltstone-dominated
Sandstone-dominated
n = 9
μ = 090°
West
East
10 m
2 m
02
03
04
05
06
07
Bedform a
Bedform a
Bedform a
Structureless
Ripple-laminated
Banded / Planar-laminated
Mudstone clast conglomerate
Bed boundary
Bedform a boundary
Erosion surface

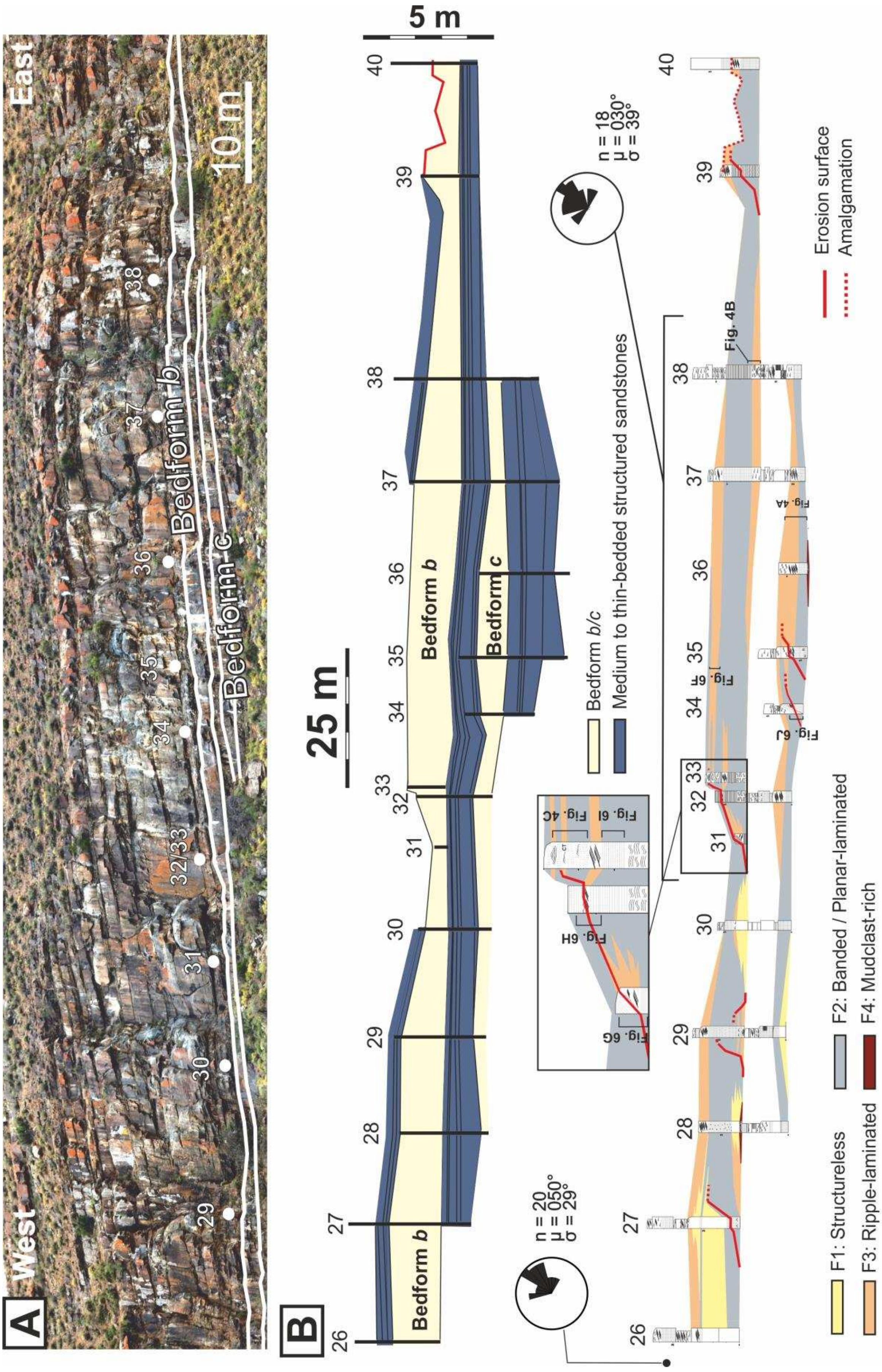
A
West
East
10 m
29
30
31
32/33
34
35
36
37
38
Bedform b
Bedform c
B
5 m
25 m
26
27
28
29
30
31
32
33
34
35
36
37
38
39
40
Bedform b
Bedform c
Bedform b/c
Medium to thin-bedded structured sandstones
n = 20
μ = 050°
σ = 29°
n = 18
μ = 030°
σ = 39°
Fig. 6G
Fig. 6H
Fig. 4C
Fig. 6I
Fig. 6J
Fig. 6F
Fig. 4A
Fig. 4B
Erosion surface
Amalgamation
F1: Structureless
F2: Banded / Planar-laminated
F3: Ripple-laminated
F4: Mudclast-rich

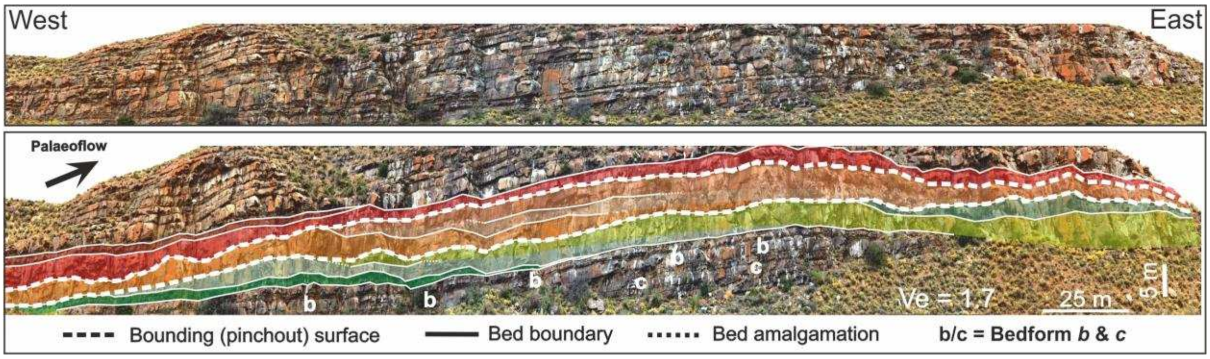
West
East
Palaeoflow
b
b
b
c
b
c
b
Ve = 1.7
25 m
5 m
Bounding (pinchout) surface
Bed boundary
Bed amalgamation
b/c = Bedform b & c

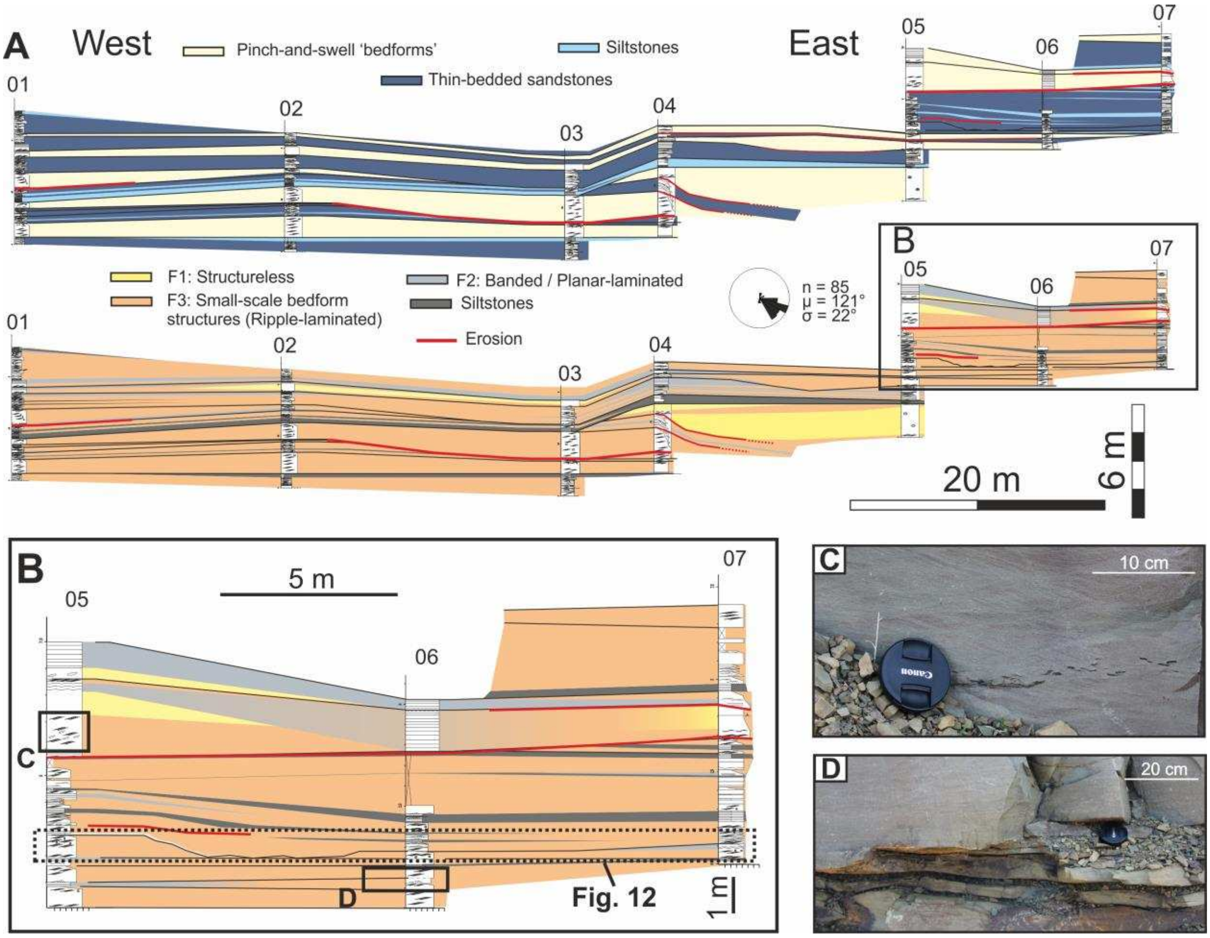
A
West
East
Pinch-and-swell 'bedforms'
Siltstones
Thin-bedded sandstones
01
02
03
04
05
06
07
F1: Structureless
F2: Banded / Planar-laminated
F3: Small-scale bedform structures (Ripple-laminated)
Siltstones
Erosion
n = 85
μ = 121°
σ = 22°
20 m
6 m
B
5 m
C
D
Fig. 12
1 m
10 cm
20 cm

1219

1220

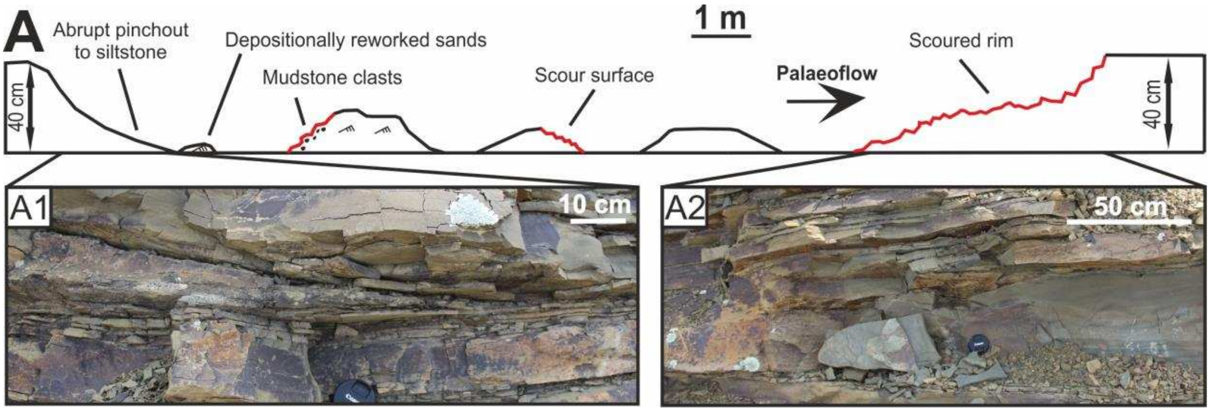
A
Abrupt pinchout to siltstone
Depositionally reworked sands
Mudstone clasts
Scour surface
1 m
Palaeoflow
Scoured rim
40 cm
40 cm
A1
10 cm
A2
50 cm

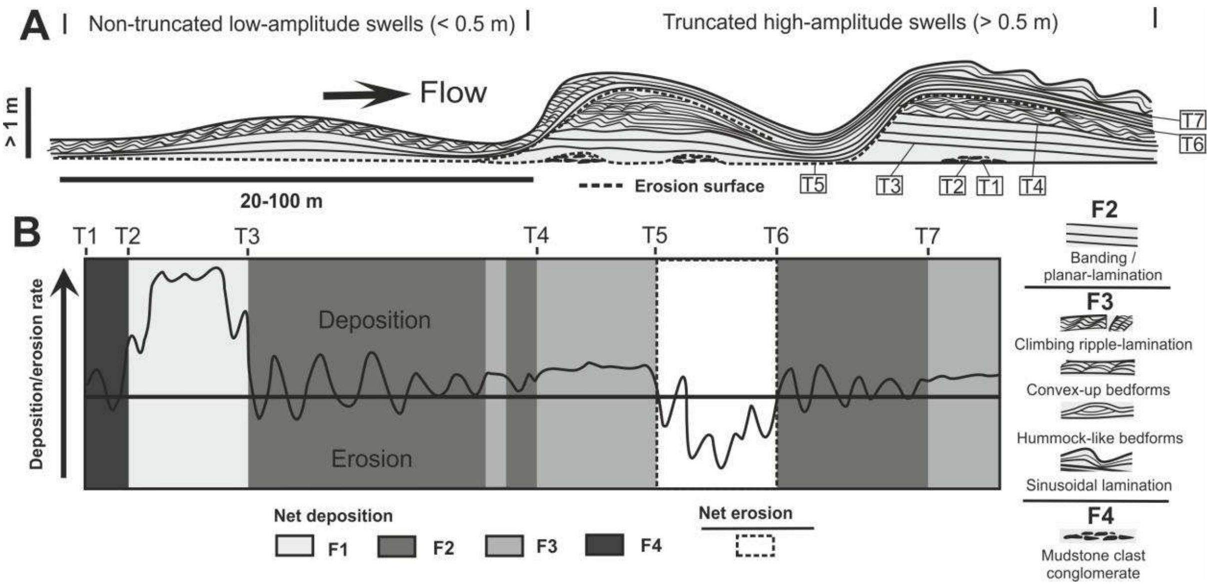

A
Non-truncated low-amplitude swells (< 0.5 m)
Truncated high-amplitude swells (> 0.5 m)
Flow
> 1 m
20-100 m
Erosion surface
T7
T6
T5
T3
T2
T1
T4
B
T1
T2
T3
T4
T5
T6
T7
Deposition/erosion rate
Deposition
Erosion
Net deposition
F1
F2
F3
F4
Net erosion
F2
Banding / planar-lamination
F3
Climbing ripple-lamination
Convex-up bedforms
Hummock-like bedforms
Sinusoidal lamination
F4
Mudstone clast conglomerate

1223

1224

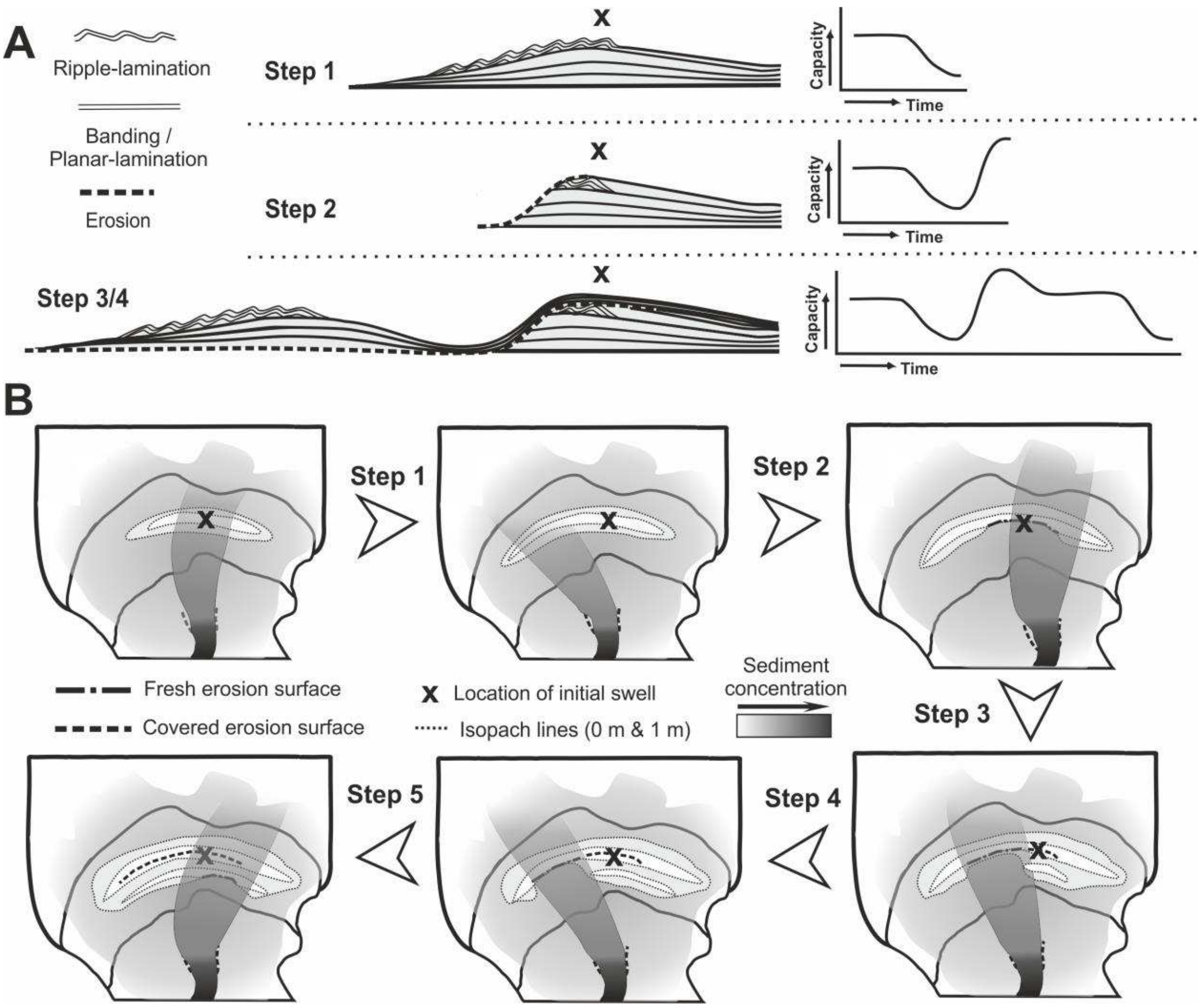
A
Ripple-lamination
Banding / Planar-lamination
Erosion
Step 1
Step 2
Step 3/4
x
Capacity
Time
B
Step 1
Step 2
Step 3
Step 4
Step 5
Fresh erosion surface
Covered erosion surface
x Location of initial swell
Isopach lines (0 m & 1 m)
Sediment concentration

1225

1226

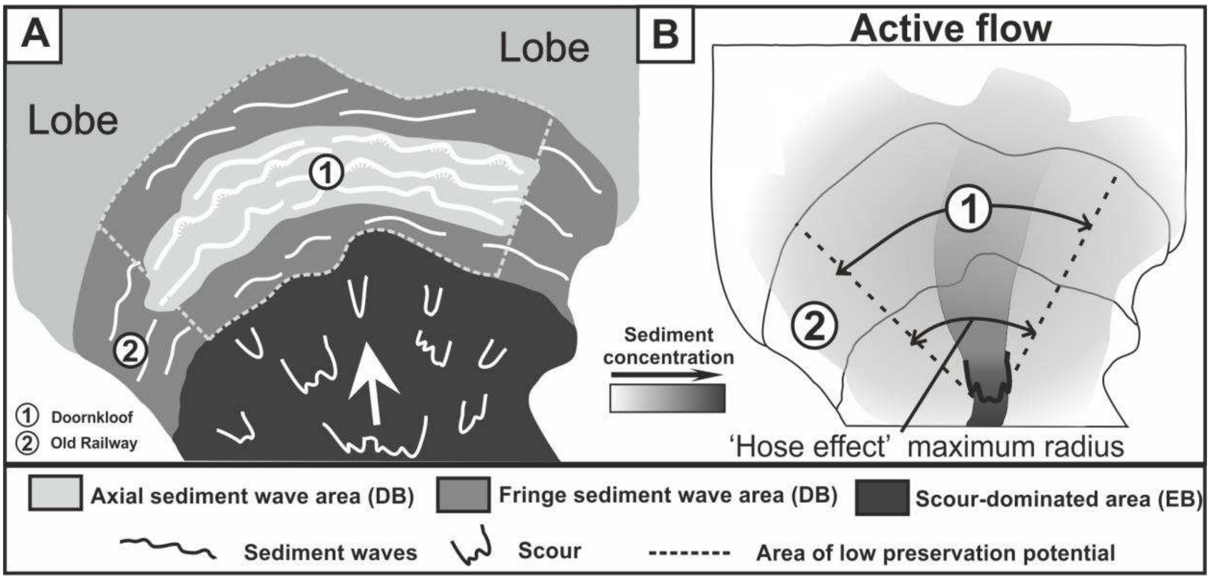
A
Lobe
Lobe
1
2
1 Doornkloof
2 Old Railway
B
Active flow
Sediment concentration
1
2
'Hose effect' maximum radius
Axial sediment wave area (DB)
Fringe sediment wave area (DB)
Scour-dominated area (EB)
Sediment waves
Scour
Area of low preservation potential

Publication	Dataset type	Formation/System	Environment	Dimensions (WL = Wavelength; CH = Crest Height)	(Average) grain size
Campion et al. (2011)	Outcrop	Cerro Toro Formation	Channel-levee	CH 1.5-15 m, WL 60-200 m	mud to very fine sand
Ito, Saito (2006); Ito (2010)	Outcrop	Boso Peninsula	Canyon	CH 0.4-2 m; WL 7-60 m	gravel
Ito et al. (2014)	Outcrop	Boso Peninsula	Canyon-mouth	CH <2 m; WL <20 m	medium to very coarse
Morris et al. (2014)	Outcrop	Laingsburg Formation	Channel-levee	CH 0.8 m; WL > 100 m	very fine sandstone
Mukti, Ito (2010)	Outcrop	Halang Formation	Channel-levee	CH 0.13 m; WL 10.7 m	mud-dominated
Piper, Kontopoules (1994)	Outcrop	Pleistocene south side Gulf of Corinth	Confined channel	CH 8 m; WL 80 m	pebbly sands to gravel
Ponce, Carmona (2011)	Outcrop	Austral foreland Basin	CLTZ	CH < 5 m, WL 10-40 m	coarse-grained
Postma et al. (2014)	Outcrop	Tabernas Basin	Canyon/channel	CH 3-8 m; WL 20-100 m	coarse sands to gravel
Vicento-Bravo, Robles (1995)	Outcrop	Albian Black Flysch	Channel-fill; CLTZ	CH 0.3-1.5 m; WL 5-40 m	pebbly sands to gravel
Winn, Dott (1977)	Outcrop	Cerro Toro Formation	Confined channel	CH <4 m; WL 8-12 m	gravel
Damuth (1979)	Modern	Manila trench	Channel-levee	CH 5-20 m; WL 300-3000 m	silt-dominated
Heinïo, Davies (2009)	Modern	Espirito Santo Basin	Channel/CLTZ	CH 10-30 m ; WL 100-300 m	coarse-grained
Howe (1996)	Modern	Barra Fan	Channel-levee	CH 5 m; WL 1750 m	silt-dominated
Kidd et al. (1998)	Modern	Stromboli Canyon	Canyon	CH 3-4m high; WL 200m long; CH 18 m, WL 800 m	sand-dominated
Lonsdale, Hollister (1979)	Modern	Reynidsjup Fan	Channel-levee	CH 20 m; WL 500 m	silt-dominated
Malinverno et al. (1988)	Modern	Var Cayon	Canyon	CH <5 m; WL 35-100 m	sand to boulders
McHugh, Ryan (2000)	Modern	Monterey Fan	Channel-levee	CH 10-25 m; WL 300-2500 m	silt-dominated
Migeon et al. (2001)	Modern	Var Fan	Channel-levee	CH 7-46 m high, WL 900-5500 m	silt-dominated
Morris et al. (1998)	Modern	Valencia Channel mouth	Channel-mouth	CH m-scale; WL 70-80 m	coarse-grained
Nakajima et al. (1998)	Modern	Toyama Fan	Channel-levee	CH <70 m; WL <3000 m	silt-dominated
Normark, Dickson (1976)	Modern	Reserve Fan	Channel-levee	WL 120-400 m	silt-dominated
Normark et al. (2002)	Modern	Hueneme Fan	Channel-levee	CH 1-8 m; WL 150 - 550 m	silt-dominated
Piper et al. (1985)	Modern	Laurentian Fan	Channel-mouth	CH 2-5 m; WL 50-100 m	gravel and gravelly sand
Praeg, Schafer (1989)	Modern	Labrador Sea	Channel-levee	CH 5-30 m; WL 500-3000 m	silt-dominated
Wynn et al. (2000a)	Modern	Selvage Fan	Channel-levee	CH <5 m, WL <1100 m	silt-dominated
Wynn et al. (2000b)	Modern	La Palma Fan	Slope/levee	CH 5-70 m; WL 400-2400 m	silt-dominated
Wynn et al. (2000b)	Modern	El Hierro Fan	Channel	CH 6m; WL <1200 m	coarse-grained